TECHNICAL REPORT STANDARD TITLE PAGE

1. Report No.	2. Government Accession No.	3. Recipient's Catalog No.
WA-RD-38.1		

4. Title and Subtitle	5. Report Date / 6. Performing Organization Code
Monitoring by Aerial and Terrestrial Photogrammetry	5. Report Date: 12/1979 6. Performing Organization Code:
7. Author(s) S. A. Veress and J. N. Hatzopoulos	8. Performing Organization Report No.
9. Performing Organization Name and Address Dept. of Civil Engineering FX-10, University of Washington, Seattle, WA 98195	10. Work Unit No. 11. Contract or Grant No.: Y-1833
12. Sponsoring Agency Name and Address Washington State Department of Transportation Highway Administration Bldg. Olympia, WA 98504	13. Type of Report and Period Covered: Final Technical Report 14. Sponsoring Agency Code

15. Supplementary Notes

This study was conducted in cooperation with the U. S. Department of Transportation, Federal Highway Administration.

16. Abstract

A photogrammetric monitoring method of structural deformation has been developed during the course of this project.

The method is based on a combination of aerial and terrestrial photographs. The theoretical experimentation for formulation of computer programs has been done on mathematical models. The combination of aerial and terrestrial photographs provides a 30% increased accuracy if compared to terrestrial photographs only. Practical experimentation was done on the existing Gabion Wall and it was indicated that the achievable accuracy is 1/120,000 of the photographic distance. The method is flexible if it can be used for monitoring of any type of structure as well as for aerial triangulation.

17. Key Words	18. Distribution Statement
Photogrammetry monitoring, simultaneous adjustment, statistical analysis and space intersection resection.	No restrictions

19. Security Classif. (of this report)	20. Security Classif. (of this page)	21. No. of Pages	22. Price
unclassified	unclassified		

Form DOT F 1700.7 (8-69)
HWY FORM 341-004 6/72

UNIVERSITY OF WASHINGTON
College of Engineering
DEPARTMENT OF CIVIL ENGINEERING

MONITORING BY AERIAL AND TERRESTRIAL PHOTOGRAMMETRY

Final Technical Report
Research Report
1979

Prepared by

S. A. Veress D.Sc., Principal Investigator

J. N. Hatzopoulos Ph.D., Research Assistant

and

Riad Munjy M.S., Graduate Student

Research conducted for Washington State Department of Transportation, in cooperation with U. S. Department of Transportation - Federal Highway Administration, under Agreement No. Y-1833

TABLE OF CONTENTS

TABLE OF CONTENTS (Continued)

LIST OF FIGURES

LIST OF FIGURES (Continued)

LIST OF TABLES

GUIDE TO NOTATION

In the following notation guide, dotted matrices are associated with the exterior orientation elements of the camera, double dots are associated with object space coordinates.

V, $\dot{V}$, $\ddot{V}$, V_i	vectors of residuals
$\dot{B}$, $\ddot{B}$, A	matrices of partial derivatives, i.e., coefficient matrices
e	accidental error
e, $\dot{e}$, $\ddot{e}$, L, J	vectors of discrepancies
ε	systematic error
$\dot{\delta}$, $\ddot{\delta}$, ΔX, X	vectors of corrections to estimates of unknown parameters
W, $\dot{W}$, $\ddot{W}$ P	weight matrices
S_p	position error
S_X, S_Y, S_Z	root mean square error of X, Y, Z
σ_i	standard error of i
Σ_{XX}	variance covariance matrix of parameters
Q_{XX}	cofactor matrix of parameters
q_{XX}	element of cofactor matrix
σ_o^2	variance factor or unit variance
r	image point radius and degrees of freedom

n	number of observations and number of points
m	number of photographs and element of M
u	number of parameters
$u, v, w,$	semiaxes of the error ellipsoid
$\lambda_1, \lambda_2, \lambda_3$	Eigen values
x, y	photographic coordinates
X_j, Y_j, Z_j	object space coordinates of point j
$X_{L_i}, Y_{L_i}, Z_{L_i}$	object space coordinates of exposure station i
M_i	unitary-orthogonal orientation matrix of the ith exposure station
ω, ϕ, κ	orientation angles
S, D	ground distances
f	focal length
K_1, K_2, K_3	radial lens distortion coefficients
$\Delta X, \Delta Y, \Delta Z$	corrections to X, Y and Z
K	atmospheric refraction coefficient
R	radius of the earth
$\dot{N}, \ddot{N}, \overline{N}_1, \overline{N}_2$	submatrices of the normal equation of bundle adjustment
$\dot{c}, \ddot{c}$	right hand side vectors of the normal equations of bundle adjustment
a_i, b_i	coefficients of the observation equations

ρ	correlation coefficient, transformation coefficient from degrees to radians
$F_1^{\frac{1}{2}}, \infty, 1-\alpha_o$	Fisher distribution value
χ^2_{α}, r	Chi square distribution value

Additional notation is defined locally within the section or sections where a particular symbol is used.

SUMMARY

The Washington State Department of Transportation in cooperation with the Federal Highway Administration sponsored a research project to develop a photogrammetric method to monitor structural deformations.

The existing photogrammetric methods for monitoring employed only terrestrial photogrammetry. This method is the combination of terrestrial and aerial photogrammetry. Therefore, this combination makes the research unique because it is the first investigation resulting in a universal solution making the method independent from terrain and the type of structure.

Because of the complicated nature of the problem, the first simulation experiments were conducted to find optimums, limitations and a standard for geometry to be applied to a mathematical process and a combination of equipment.

This mathematical simulation proved that the combination of aerial and terrestrial photogrammetry is feasible. The desirable geometry is a parallactic angle which should be about 60 degrees. The aerial photographs should be tilted so that a 90 degree intersecting angle will not be made on the terrestrial photographs. The maximum angular limit that is permissible is 85 degrees. This limit permits the use of conventional aerial cameras for certain structures such as bridges.

The mathematical solution, as shown by the simulation experiments, should be adjusted in two steps: first the sequential adjustment for primary estimate values and second a final simultaneous adjustment.

The achievable accuracy of the combined systems indicate a 50%

improvement over the terrestrial photogrammetric method.

These practical experiments have been obtained using the I-90 Gabion Wall as a structure. The structure was photographed from the ground by a modified KA-2 terrestrial camera and from the air by a Wild and later by an Aero-View f=6" camera.

Theoretical predictions concerning accuracy influences various types of geometric factors which prove to be correct. The accuracy that was achieved by this practical experiment is 1/120,000 of the photographic distance. This represents a substantial improvement over the accuracy achieved by terrestrial photogrammetry alone.

Computer programs have been developed for this research to perform the task of mathematical processing. These computer programs are excluded from this presentation because it has been transmitted to the Washington State Department of Transportation Photogrammetric Branch and is already in use in their computers.

INTRODUCTION

1.1 Background Studies

In 1968, through the sponsorship of the Washington Highway Department and the Bureau of Public Roads, a research project was initiated to determine whether or not motion and deflection of retaining walls could be determined by photogrammetric methods (Veress, 1971a). The research results indicated that the photogrammetric monitoring method is capable of providing the required accuracy. Similar projects have been implemented in Canada (Erez, 1971, Brandenberger and Erez, 1972), in West Germany (Planicka, 1970) and Romania (Grutu, 1972). The U. S. Corps of Engineers, Seattle District, realizing the economical and technical potential of analytical terrestrial photogrammetry, began various investigations in 1970 to establish their method for routine applications (Erlandson, Peterson and Veress, 1973, 1974a; Erlandson and Veress, 1974a, 1975, 1976).

The Washington State Highway Department in conjunction with the Federal Highway Administration, had sponsored a research project 1975-1977 to monitor the motion of a gabion wall (Flint, 1975; Sun, 1976; Veress, Hou, 1977; Veress and Sun, 1978; Veress, Jackson and Hatzopoulos, 1979). The accuracy obtained in that project was 1:85,000 of an 850 m assumed photographic distance (Veress, Hou, 1977). The results obtained were found to be compatible to data obtained by an inclinometer (Veress, Jackson and Hatzopoulos, 1979).

The Washington State Highway Department offered a research project 1977-1979 for further investigation in the photogrammetric monitoring field by developing a universal method which in the case of a large structure will employ a combination of aerial and terrestrial photography. The method will also be based on a rigorous analytical solution providing full statistical analysis.

1.2 Problem Statement

A search of the current literature reveals that the present state-of-the-art in photogrammetric monitoring of structures is basically as follows: Some of the cases utilize sequential non-rigorous adjustment methods based on classical aerial triangulation. There is one case where a rigorous solution is applied (Erlandson and Veress, 1975). This is based on field measurements of the exterior orientation parameters, however, the computer algorithm for this requires a large amount of core storage and a significant amount of processing time in a high speed computer, to make a simultaneous adjustment for only a limited number of points. The existing research in structural deformation measurement by photogrammetry is limited to either strictly terrestrial photography or strictly aerial photography which is employed in the same manner as for traditional aerial triangulation. This research, however, utilizes a combination of terrestrial and aerial photography, thus giving the flexibility to the designer so as to obtain the optimum geometry of the surveying system even when terrain features do not permit a favorable location of the terrestrial platforms. The analysis of data from a simulation experiment established that there are required limits for creating optimum geometry for various combinations of terrestrial and aerial photography. The bundle method, which is generally adopted for analtyical photogrammetric applications, is used in this research in an appropriate manner so as to give a rigorous solution based on comparator observations and minimizing the ground surveys. The minimum ground control can comprise only one measured distance not necessarily with high precision (see Ch. III). The desirable ground survey is to determine precisely three control points. The developed adjustment method in this research is very economical requiring a relatively small amount of computer core storage memory (less than 77K in the University of Washington Cyber 73/CDC 6400 computer) and a relatively small amount of computer time. The costs in this method do not increase significantly by increasing the number of the points. This method utilizes all parameters as observations with a priori assigned variances, thus enabling a full statistical analysis of the final results. In this research a method to detect observation blunders is also indicated, particularly when an inexpensive camera is used. The practical evaluation of four sets of actual data in a three year period of time, which includes aerial photography, has indicated a relative accuracy of 1:120,000 of the assumed photographic distance.

2.0 SIMULATED MODEL FOR GEOMETRICAL EFFICIENCY

2.1 A Simulation Experiment

It was necessary, during the course of this research project, to study the effect of various parameters on achievable accuracy. While the best practical solution is to obtain actual examples, this could not be conducted here because of the high cost due to the large number of parameters involved. Therefore, a mathematical model was developed first. Several simulation experiments were conducted to find the most desirable geometry, the effect of various types of error and finally to establish a standard for the photogrammetric design. Once this goal has been achieved then it is verified by a practical example.

The simulation experiment begins by generating fictitious photogrammetric data which is obtained in a mathematical manner of combinations of aerial and terrestrial photography. The fictitious model, however, is based on a mathematical test area which has been chosen so as to express a generalized surface, similar to a hillside. The selected mathematical area is shown in planimetric view in Fig. 2.1 and in isometric view in Fig. 2.2 and 2.3. The hypothetical test area has dimensions of 2000 feet by 2000 feet. It includes 99 points whose mathematical coordinates are given in Table 2.1. The location of the ground points (Fig. 2.1) is according to a grid pattern in order to cover the whole test area uniformly. The simulated cameras have been selected to have an image format 9-1/2 by 9-1/2 inches and focal lengths of 24 inches for the terrestrial camera, 6 inches for the aerial camera. These camera constants are the same as for the actual test area. The mathematical test area is "photographed" from two or three different

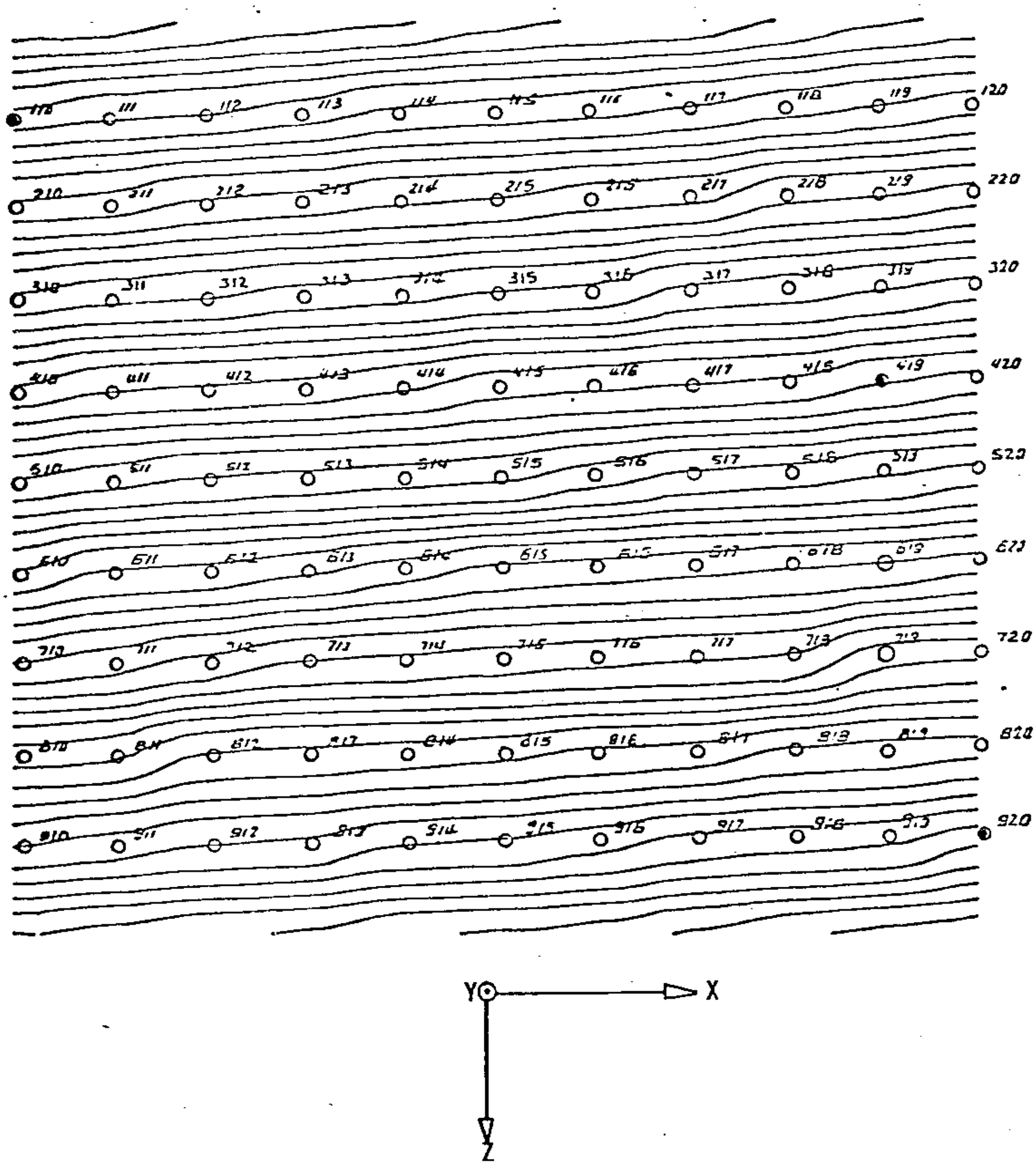

Fig. 2.1. The mathematical area (planimetric view) contour interval 20'.

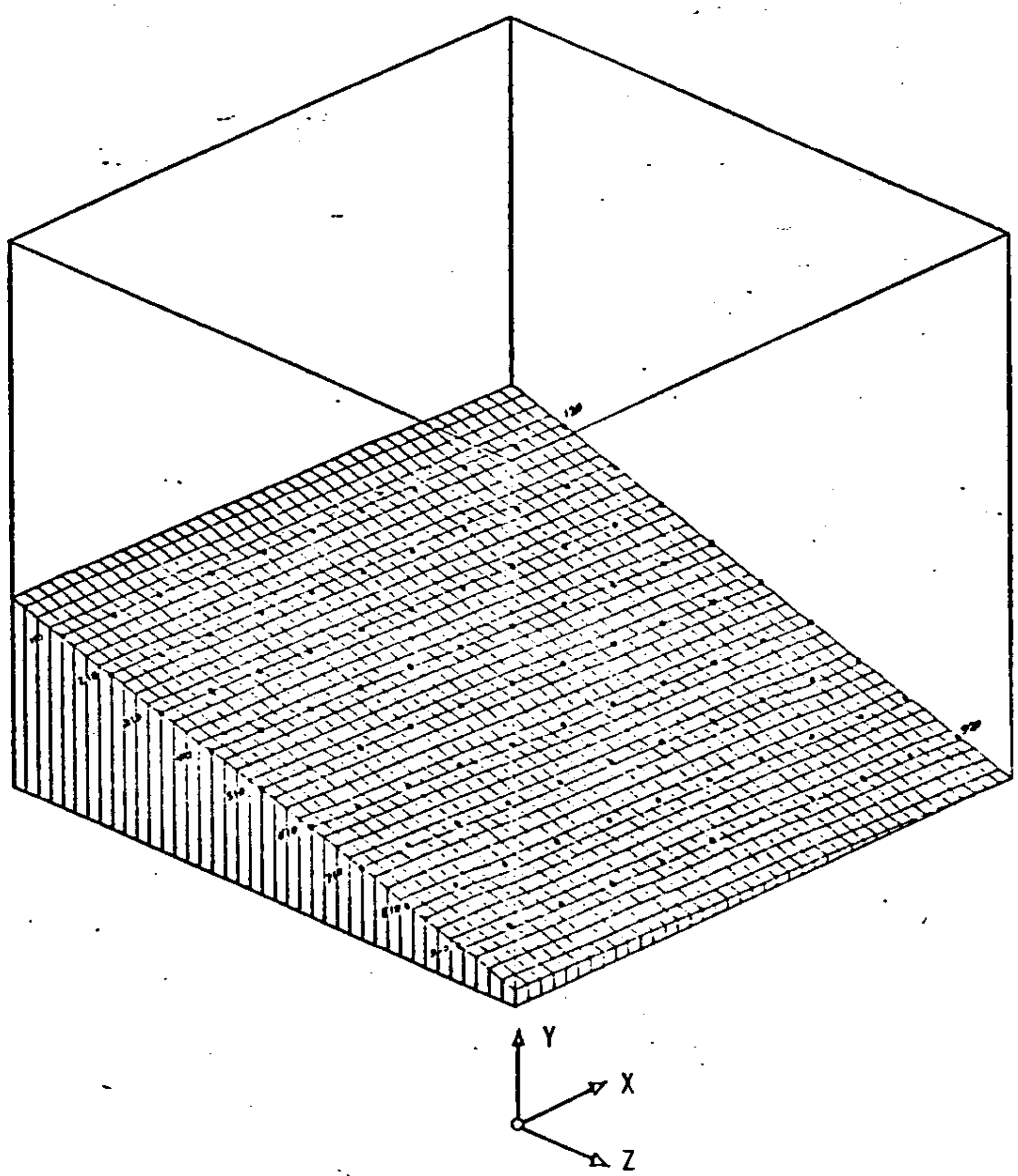

Fig. 2.2. The mathematical area (left view).

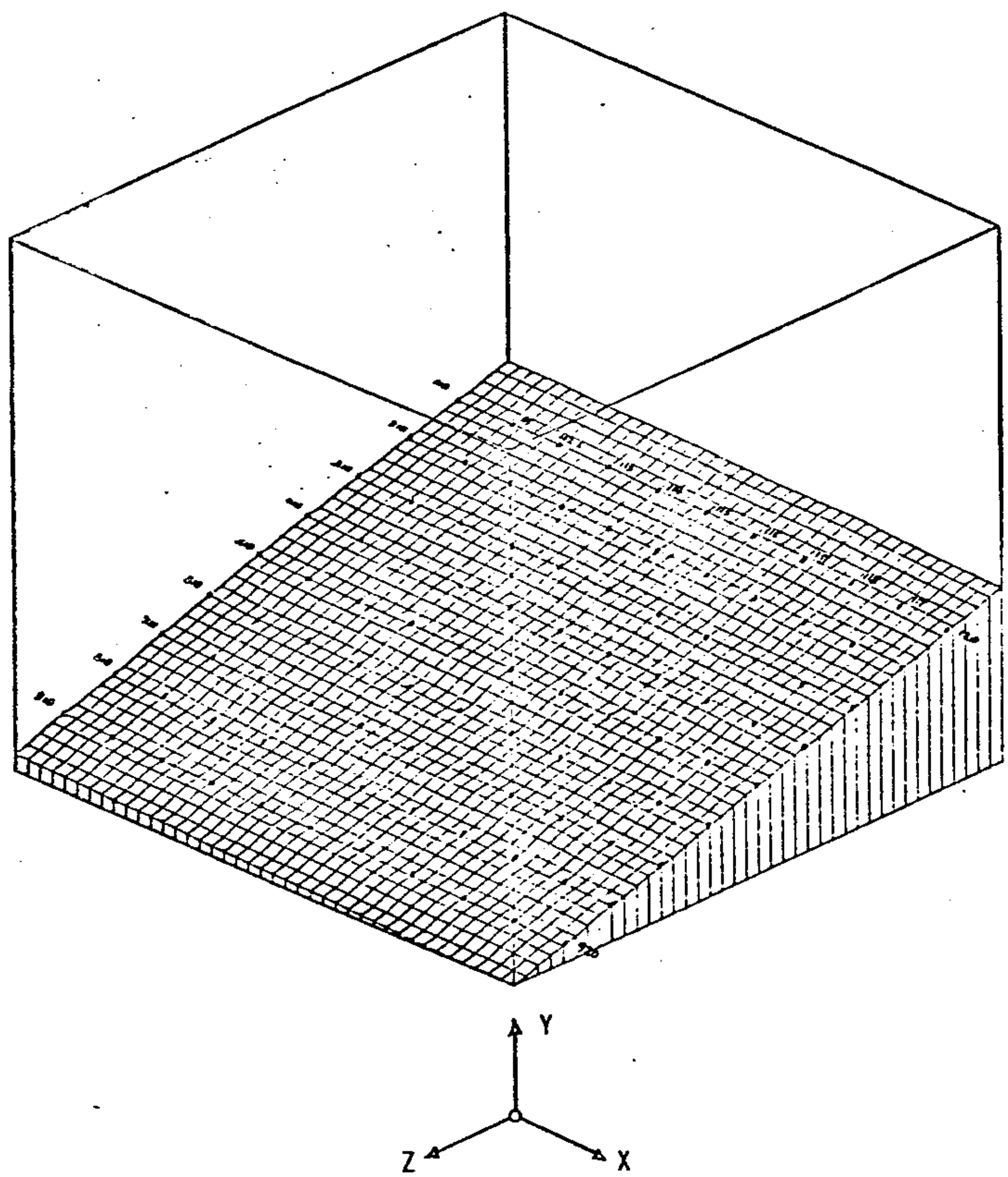

Fig. 2.3. The mathematical area (right view).

stations. When two stations are used they are assumed to be both terrestrial, when three stations are used the third one is assumed to be an aerial platform.

2.2 Definition of the Parallactic Angle.

The geometry for the photogrammetric survey can be expressed in terms of the parallactic angles. The term terrestrial parallactic angle used here expresses the angle of intersection between the optical axes of the two terrestrial cameras at the mean plane containing the targets (see Fig. 2.4).

The parallactic angle for the aerial camera, or the aerial parallactic angle, is defined here as the angle between the axis of the aerial camera and the horizontal plane. Fig. 2.4 illustrates the adopted parallactic angle concept. The importance of the parallactic angle in photogrammetric monitoring surveys has been pointed out by Erlandson and Veress, 1975 as being significant for determining the precision of the coordinates of an intersected object point. It must be emphasized that near-zero parallactic angles create typically unfavorable intersections, while parallactic angles close to 90° create strong intersection geometry. This simulation experiment also investigates limitations of the parallactic angle when using combination of aerial and terrestrial photography. The location of a camera in terms of exterior orientation elements is determined by the coordinates X_L, Y_L, Z_L of the frontal nodal point of the camera lens with reference to a ground coordinate system of X, Y, Z and by the three rotational angles which are defined as ω-rotation about the X axis, ϕ-rotation about the Y axis and κ-rotation about the Z axis. Assuming $\kappa' \approx \kappa'' \approx 0$ and $\omega' \approx \omega''$ the

Table 2.1. Three-dimensional coordinates of ground points (feet).

Point No	X	Y	Z	Point No	X	Y	Z
110	1000	1900	-2600	516	2200	1450	-1800
111	1200	1890	-2600	517	2400	1435	-1800
112	1400	1885	-2600	518	2600	1430	-1800
113	1600	1875	-2600	519	2800	1420	-1800
114	1800	1860	-2600	520	3000	1410	-1800
115	2000	1855	-2600				
116	2200	1850	-2600	610	1000	1400	-1600
117	2400	1840	-2600	611	1200	1380	-1600
118	2600	1830	-2600	612	1400	1375	-1600
119	2800	1820	-2600	613	1600	1365	-1600
120	3000	1810	-2600	614	1800	1350	-1600
210	1000	1800	-2400	615	2000	1335	-1600
211	1200	1795	-2400	616	2200	1330	-1600
212	1400	1780	-2400	617	2400	1325	-1600
213	1600	1775	-2400	618	2600	1320	-1600
214	1800	1765	-2400	619	2800	1315	-1600
215	2000	1760	-2400	620	3000	1305	-1600
216	2200	1750	-2400	710	1000	1300	-1400
217	2400	1745	-2400	711	1200	1290	-1400
218	2600	1725	-2400	712	1400	1275	-1400
219	2800	1720	-2400	713	1600	1260	-1400
220	3000	1710	-2400	714	1800	1255	-1400
310	1000	1700	-2200	715	2000	1250	-1400
311	1200	1690	-2200	716	2200	1245	-1400
312	1400	1685	-2200	717	2400	1240	-1400
313	1600	1675	-2200	718	2600	1235	-1400
314	1800	1670	-2200	719	2800	1205	-1400
315	2000	1660	-2200	720	3000	1200	-1400
316	2200	1655	-2200	810	1000	1190	-1200
317	2400	1635	-2200	811	1200	1185	-1200
318	2600	1630	-2200	812	1400	1160	-1200
319	2800	1620	-2200	813	1600	1155	-1200
320	3000	1610	-2200	814	1800	1150	-1200
410	1000	1600	-2000	815	2000	1145	-1200
411	1200	1585	-2000	816	2200	1135	-1200
412	1400	1580	-2000	817	2400	1130	-1200
413	1600	1575	-2000	818	2600	1115	-1200
414	1800	1565	-2000	819	2800	1110	-1200
415	2000	1550	-2000	820	3000	1105	-1200
416	2200	1545	-2000	910	1000	1100	-1000
417	2400	1540	-2000	911	1200	1090	-1000
418	2600	1535	-2000	912	1400	1080	-1000
419	2800	1520	-2000	913	1600	1075	-1000
420	3000	1510	-2000	914	1800	1060	-1000
510	1000	1500	-1800	915	2000	1055	-1000
511	1200	1490	-1800	916	2200	1045	-1000
512	1400	1480	-1800	917	2400	1030	-1000
513	1600	1475	-1800	918	2600	1025	-1000
514	1800	1470	-1800	919	2800	1020	-1000
515	2000	1465	-1800	920	3000	1000	-1000

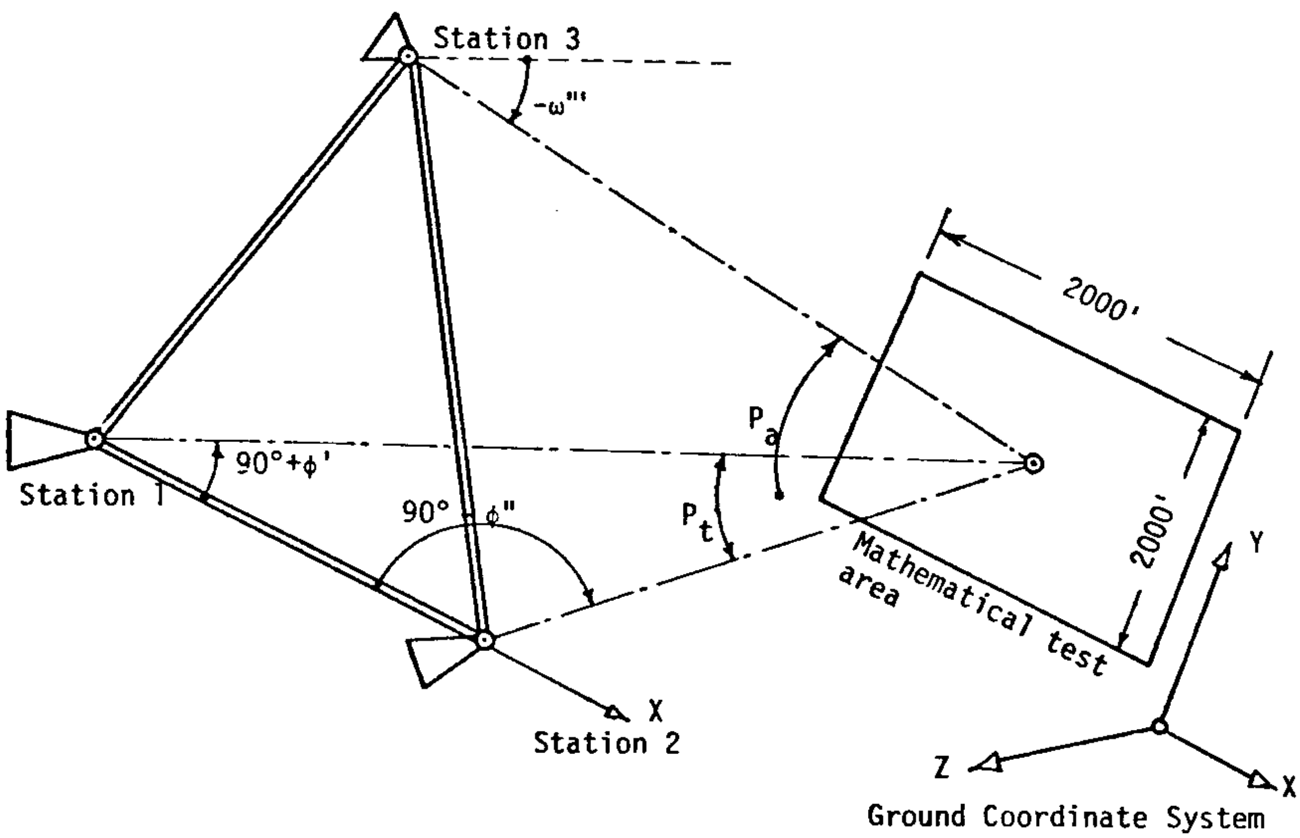

Fig 2.4. Definition of the mathematical test area.
P_t: is the terrestrial parallactic angle.
P_a: is the aerial parallactic angle.

terrestrial parallactic angle is then defined as follows (see Fig. 2.4):

$$P_t = \phi'' - \phi'$$

Where ω', ϕ', κ' are the rotation angles for the left camera.

ω'', ϕ'', κ'' are the rotation angles for the right camera.

Assuming $\kappa''' \approx 0$, $\phi''' \approx 0$, then the aerial parallactic angle is defined as follows (see Fig. 2.4):

$$P_a = -\omega'''$$

Where ω''', ϕ''', κ''' are the ω, ϕ, κ rotations for the aerial camera.

2.3 Combination of Camera Stations

The simulation experiment utilizes three different terrestrial parallactic angles and three different aerial parallactic angles. The terrestrial parallactic angles are chosen to be: 30°, 60°, 90°. The aerial parallactic angles are selected to be 82°, 60° and 30°. By using only two terrestrial stations, three additional combinations are obtained. The simulation experiment, therefore, has a total of twelve camera configurations with different geometric features. The values of the exterior orientation elements for each combination are given by Table 2.2. The assumed mathematical values are applied to Equations

$$x_{ij} = -f_i \frac{M_{1i}X_{ij}}{M_{3i}X_{ij}}, \quad y_{ij} = -f \frac{M_{2i}X_{ij}}{M_{3i}X_{ij}}$$

and the x_{ij}, Y_{ij} fictitious image coordinates are computed.

2.4 Process of the Simulation Experiment.

The computation phase of the experiment is performed by a sequential intersection program which is based on the "vector method".

Table. 2.2. Values of exterior orientation elements of various camera stations.

Combination No	Camera St. No	X_L Feet	Y_L Feet	Z_L Feet	ω Degrees	φ Degrees	κ Deg.
1	1 2 3	240 3760 2015	1455 1460 3250	+4770 +4765 -1550	0 0 -82	-15 +15 0	0 0 0
2	1 2 3	-1500 5500 2018	1471 1468 3020	+4250 +4260 -905	0 0 -60	-30 +30 0	0 0 0
3	1 2 3	-3020 7020 2005	1480 1475 2360	+3220 +3230 -240	0 0 -30	-45 +45 0	0 0 0
4	1 2 3	240 3760 2018	1455 1460 3020	+4770 +4765 -905	0 0 -60	-15 +15 0	0 0 0
5	1 2 3	-1500 5500 2005	1471 1468 2360	+4250 +4260 -240	0 0 -30	-30 +30 0	0 0 0
6	1 2 3	-3020 7020 2015	1480 1475 3250	+3220 +3230 -1550	0 0 -82	-45 +45 0	0 0 0
7	1 2 3	240 3760 2005	1455 1460 2360	+4770 +4765 -240	0 0 -30	-15 +15 0	0 0 0
8	1 2 3	-1500 5500 2015	1471 1468 3250	+4250 +4260 -1550	0 0 -82	-30 +30 0	0 0 0
9	1 2 3	-3020 7020 2018	1480 1475 3020	+3220 +3230 -905	0 0 -60	-45 +45 0	0 0 0
10	1 2	240 3760	1455 1460	+4770 +4765	0 0	-15 +15	0 0
11	1 2	-1500 5500	1471 1468	+4250 +4260	0 0	-30 +30	0 0
12	1 2	-3020 7020	1480 1475	+3220 +3230	0 0	-45 +45	0 0

The input data are:

a. The exterior orientation elements as given by Table 2.2

b. The fictitious image coordinates

c. Several types of perturbation errors introduced to the fictitious image coordinates.

The output data are:

a. The computed ground coordinates for all the points within the test area.

b. The differences V_{Xi}, V_{Yi}, V_{Zi} which are defined as:

$$V_{Xi} = X_m - X_c$$

$$V_{Yi} = Y_m - Y_c$$

$$V_{Zi} = Z_m - Z_c$$

Where the index i refers to any of the ninty-nine points which are included within the mathematical test area. X_m, Y_m, Z_m are the ground coordinates given by Table 2.1. X_c, Y_c, Z_c are the computed ground coordinates obtained via the intersection program.

c. The mean square value of the differences defined as:

$$S_x = \sqrt{\frac{[V_{Xi}V_{Xi}]}{n}}$$

$$S_y = \sqrt{\frac{[V_{Yi}V_{Yi}]}{n}}$$

$$S_z = \sqrt{\frac{[V_{Zi}V_{Zi}]}{n}}$$

Where n is the number of ground points in the formula above, the symbol $[V_i\ V_i]$ indicates $\sum_{i=1}^{n} V_i^2$

d. The algebraic sum of the differences defined as

$$\Sigma_X = \sum_{i=1}^{n} V_{Xi}$$

$$\Sigma_Y = \sum_{i=1}^{n} V_{Yi}$$

$$\Sigma_Z = \sum_{i=1}^{n} V_{Zi}$$

The errors which are introduced to the fictitious image coordinates are:

a. Rounding off errors. This error is present in all fictitious image coordinates since the least significant figure is rounded to the nearest μm.

b. Systematic error in terms of residuals from the lens distortion correction function. In this the photograph is divided by the axes of the image coordinate system into four quarters (Fig.2.5). Each quarter of the photograph is assumed to have a different distortion curve. The lens distortion error is introduced to the image coordinates according to which quarter of the photograph, they are located.

All image coordinates are then corrected by the average of the four lens distortion curves. The lens distortion coefficients, as taken from the calibration data of a Wild RC5/RC8 camera, are given in Table 2.3. The lens distortion curve is assumed to be expressed by the equation:

$$\Delta r = K_1 r + K_2 r^3 + K_3 r^5$$

Where Δr is the amount of radial displacement of a point in a photograph due to the lens distortion. K_1, K_2, K_3 are distortion coefficients, r is the radial distance from the principal point to the photographic image point.

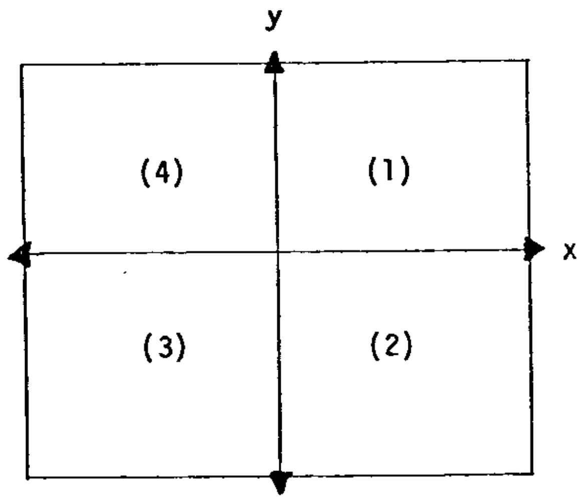

Fig. 2.5 Subdivision of the photograph (positive plane) into four quarters with each quarter having different lens distortion coefficients.

c. Random error. Random or accidental error is introduced up to a magnitude of six micrometres in the image coordinates. Table 2 .4 gives the values of the accidental error in micrometres.

For the first nine combinations (see Table 2. 3), there are three independent computations of the intersection program. The first computation uses the fictitious image coordinates with round-off error only. The second computation used the round-off values of the image coordinates plus the residuals from the lens distortion corrections. Finally, the image coordinates used for the third computation have all the errors introduced in the second computation plus the acci-

Table 2.3 Lens distortion coefficients

			Remarks
1st Quarter	K_1	4.868965×10^{-2}	Distortion coefficents used to generate distortion error to the fictitious image coordinates
	K_2	-2.570416×10^{-5}	
	K_3	1.356176×10^{-9}	
2nd Quarter	K_1	5.124368×10^{-2}	
	K_2	-2.642100×10^{-5}	
	K_3	1.387325×10^{-9}	
3rd Quarter	K_1	1.193063×10^{-1}	
	K_2	-2.973802×10^{-5}	
	K_3	1.357450×10^{-9}	
4th Quarter	K_1	8.246735×10^{-2}	
	K_2	-3.218110×10^{-5}	
	K_3	1.647088×10^{-9}	
Average of all four quarters	K_1	7.608910×10^{-2}	Distortion coeffi-cient used to correct the lens distortion error
	K_2	$-2,877316 \times 10^{-5}$	
	K_3	1.452724×10^{-9}	

dental errors as they are given by Table 2.4. In Table 2.4, the errors listed in the columns x_1, y_1, are introduced to the x, y image coordinates of the left terrestrial photograph, the errors of the columns x_2, y_2, are for the right terrestrial photograph, the errors of the columns x_3, y_3, are for the aerial photograph.

The purpose of the first computation is to study the effect of round-off error, the purpose of the second computation is to study the effect of systematic error, and the reason for the third computation is to study the effect of accidental error.

For the last three combinations (see Table 2.2) only the third computation is performed.

In the simulation experiment, however, a total of (3 x 9 + 3 = 30) independent computations of the intersection program are performed combining different geometric features of the mathematical model and introducing different types of errors in the input image coordinates.

2.5 Evaluation of the Simulation Experiment.

The output data obtained by the intersection computer program are listed in the Tables 2.5 through 2.9.

The Table 2.5 represents the effect of round-off error. This effect seems to be most pronounced in the z direction. In terms of photographic distance, which is taken as being 7,100 feet, if this is the only existing error, it yields relative accuracy of 1/1,420,000. It is considered this will have a minimal effect on the final coordinates in terms of the desired final accuracy of 1/100,000 of the photographic distance. The differences V_{Xi}, V_{Yi}, V_{Zi} are greater for points

Table 2.4. Accidental error in micrometre.

N.P.	x_1	y_1	x_2	y_2	x_3	y_3	N.P.	x_1	y_1	x_2	y_2	x_3	y_3
1	-5	-1	-2	-1	-2	0	51	3	-5	-5	-4	-2	-2
2	6	-1	6	0	-4	-5	52	-6	3	-1	5	2	-1
3	-1	4	3	2	-6	-4	53	-2	5	4	-2	0	4
4	-5	-2	2	4	-5	-2	54	3	1	5	5	1	-2
5	0	-5	5	-4	-4	5	55	-4	-6	-5	-1	-2	0
6	0	4	2	6	-2	2	56	-6	-6	4	3	-4	3
7	-2	-1	-5	-1	-5	-3	57	0	-2	5	5	-2	-1
8	0	2	-5	-4	1	6	58	2	-1	-2	2	-1	-6
9	6	-6	5	6	6	1	59	6	-1	4	6	-6	2
10	5	0	5	-3	4	5	60	-2	1	2	-4	-4	3
11	-2	4	-1	-2	1	-4	61	5	0	-3	0	6	5
12	-6	0	-6	0	3	4	62	2	-5	-5	0	6	4
13	-2	2	4	4	4	4	63	1	4	-4	4	5	5
14	3	1	1	-6	-5	-5	64	-3	-4	3	5	-2	6
15	-4	6	5	-6	3	2	65	-2	5	3	2	4	-2
16	0	3	-6	-3	3	0	66	-2	5	6	5	4	5
17	1	4	-6	1	-2	-4	67	5	0	-6	-3	5	-2
18	6	4	0	5	-6	-2	68	4	-1	4	-1	0	0
19	-1	-2	5	0	-5	4	69	-6	2	-1	-4	6	-4
20	2	1	1	-1	-3	5	70	4	-1	-6	2	6	6
21	-3	1	6	1	1	-5	71	-2	1	3	-6	5	4
22	3	-5	5	2	-6	-3	72	5	3	0	5	6	-6
23	1	3	5	4	-2	4	73	-2	6	3	-5	-4	5
24	-2	0	-5	5	1	1	74	-3	6	5	-2	5	4
25	2	-2	-2	6	-4	-1	75	-6	2	1	6	3	-4
26	6	0	6	6	0	-5	76	1	-4	1	-4	4	-6
27	-5	0	6	1	5	3	77	-3	-3	0	-3	5	-1
28	-6	3	-4	4	6	2	78	-6	5	-2	4	-4	-6
29	-5	-2	1	-4	5	5	79	-3	6	2	3	2	-6
30	0	3	5	-6	0	-4	80	-2	-5	-1	3	5	-1
31	6	5	-1	4	0	0	81	4	0	5	-3	0	4
32	2	-6	-6	-4	-1	4	82	4	0	3	0	6	6
33	0	-2	-3	3	2	-6	83	-6	-1	-1	-4	5	-6
34	-2	0	1	6	-1	-6	84	-5	4	4	-5	3	-6
35	1	-6	0	-1	5	-6	85	4	-1	-1	-2	0	-6
36	3	5	5	0	-4	0	86	5	0	6	-2	0	-6
37	-3	5	-6	5	-3	-6	87	-1	-2	4	-6	1	-1
38	2	5	-4	5	5	-3	88	2	1	4	1	4	-4
39	-6	5	4	1	1	4	89	-4	-5	-6	1	1	-5
40	3	-5	6	2	-6	3	90	-2	-2	6	2	5	-5
41	2	6	0	-6	-2	-6	91	-2	-2	-4	2	2	-1
42	-6	3	-6	5	1	0	92	-1	0	2	2	1	-6
43	-6	-4	-6	-3	-2	-1	93	4	6	2	5	-6	1
44	2	-2	-1	-4	-6	6	94	-5	-4	4	4	-2	-6
45	5	-6	6	-2	-5	2	95	-4	5	4	-4	1	-4
46	-1	3	-5	2	0	-5	96	-1	5	1	-4	-1	0
47	3	6	1	2	-1	3	97	-6	-6	-4	-4	-6	5
48	-3	1	0	5	5	-2	98	3	-5	-4	5	0	0
49	2	-6	-4	-4	5	-3	99	-1	1	-4	3	1	-5
50	-4	1	3	3	-3	3							

located away from the center of the test area. The Σ_{VX}, Σ_{VY}, Σ_{VZ} are very small and tests have indicated that there is no systematic error.

The Table 2.6 represents the systematic error effect. The values in the Σ_{VX}, Σ_{VY}, Σ_{VZ} columns are large and tests indicate that the residuals composing the corrections to the lens distortion have systematic error. The X-direction seems to be subject to the greatest effect of error because the points on the photograph are scattered along the X-axis.

The residuals in terms of image coordinates, are either near zero or about one micrometre in value. For points close to the edge of the photograph, the magnitudes become 2 or 3 micrometres. The lens distortion residuals yield relative accuracy 1/400,000. This is a small effect but it cannot be neglected. It is appropriate, however, to correct the distortion so that the residuals do not exceed a few micrometres.

The Table 2.7 represents the effect of all types of error. The greatest effect is due to the accidental errors which have been introduced to the image coordinates up to a maximum value of 6μm. The columns Σ_{VX}, Σ_{VY}, Σ_{VZ} show the inherent systematic errors from the lens distortion residuals as compared with those listed in Table 2.6.

The largest effect of accidental errors is in the Z-direction, this being about 50% larger than the effect in the X and Y directions.

The accuracy which can be achieved considering all error effects is 1:122,000 of the photographic distance. This also yields information about the maximum accuracy which can be obtained in the determination of the absolute position of a point in the three dimensional space for

Table 2.5. Rounding error (1/1000 feet).

Comb. No.	S_X	S_Y	S_Z	ΣV_X	ΣV_Y	ΣV_Z
1	2	2	3	31	-15	1
2	2	2	3	-1	22	12
3	2	2	3	-2	-21	10
4	2	2	5	-28	-5	-4
5	2	2	4	2	5	13
6	2	2	2	-9	-13	20
7	2	2	6	-37	-20	-34
8	2	2	3	-3	16	15
9	2	2	3	-8	-6	17

Table 2.6. Systematic error (1/1000 feet).

Comb. No.	S_X	S_Y	S_Z	ΣV_X	ΣV_Y	ΣV_Z
1	12	5	10	-824	209	338
2	13	5	10	-842	268	382
3	12	5	7	-822	253	315
4	12	5	10	-809	238	360
5	12	5	9	-801	267	290
6	14	5	9	-968	242	408
7	12	6	10	-812	254	226
8	13	5	9	-872	242	369
9	13	5	9	-911	271	407

Table 2.7. Accidental error (1/1000 feet).

Comb. No.	S_X	S_Y	S_Z	ΣV_X	ΣV_Y	ΣV_Z
1	28	31	49	-1044	-283	736
2	31	29	46	-1096	-103	516
3	34	27	39	-1129	87	159
4	29	30	58	-1063	-180	822
5	31	27	52	-1059	64	207
6	35	30	35	-1268	-226	366
7	31	27	84	-1085	-26	451
8	31	31	41	-1110	-235	459
9	35	28	37	-1217	-77	401

Table 2.8. Accidental error for terrestrial cameras (unit 1/1000 feet)

Comb. No.	s_X	s_Y	s_Z	Σv_X	Σv_Y	Σv_Z
10	37	31	110	-939	-202	-1623
11	40	32	59	-1006	-181	-599
12	50	32	43	-1199	-192	-319

Table 2.9. Position error (unit 1/1000 feet)

Comb. No.	Accidental Error S_p	Terrestrial Parallactic Angle (Degr.)	Aerial Parallactic Angle (Degr.)	Relative Precision %
1	64	30	82	91
2	63	60	60	92
3	58	90	30	100
4	72	30	60	81
5	66	60	30	88
6	58	90	82	100
7	93	30	30	62
8	60	60	82	97
9	58	90	60	100
10	120	30	-	48
11	78	60	-	74
12	73	90	-	79

the chosen geometry.

The structural deformation, as measured by photogrammetry, does not refer to an absolute coordinate system as the present application. But it takes the first set of measurements as the origin which is then considered to have no structural deformation. The second set of measurements may exhibit structural deformation and the difference of the spatial coordinates between the two sets indicates the vector of the structural motion. It is, however, possible for all sets to have the same systematic error, which in terms of absolute position of a point, could be a significant influence. But, in terms of structural deformation, such an error is of limited concern.

The Table 2.8 represents all error effects in the case where only two terrestrial cameras are used. This data is presented in order to show that when using only two cameras the anticipated accuracy decreases because of the weakened geometry.

Finally, Table 2.9 gives the position error for all combinations. The position error is defined as:

$$S_p = \pm \sqrt{S_X^2 + S_Y^2 + S_Z^2}$$

The last column of Table 2.9 indicates the relative precision for each parallactic angle group, as compared to those groups which provide the minimum position error. The minimum position error is provided by the combination No. 3, No. 6 and No. 9 and, therefore, a relative precision of 100% is assigned to them. The position error is plotted versus the parallactic angle (Fig. 2.6) and this graph also indicates the limits of the parallactic angle for a desirable geometry. The

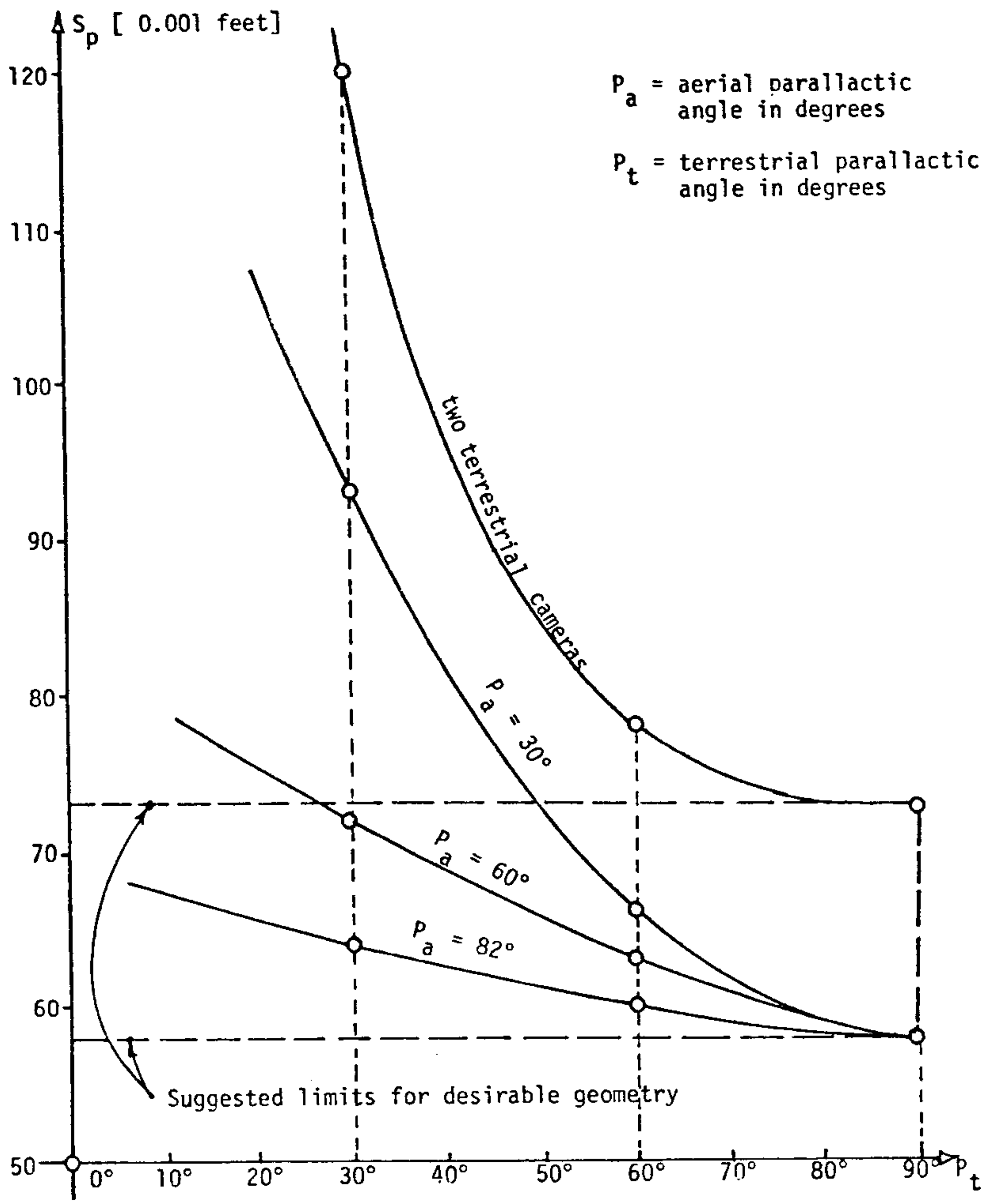

Fig. 2.6. Analysis of the position error effect by introducing all types of error to the image coordinates.

geometric properties of the mathematical model can be also studied in relation to the relative precision given in Table 2.9.

In this simulation experiment, however, the combination No. 3, No. 6 and No. 9 provides the best geometry while the combination No. 2, No. 5 and No. 8 yields close to the optimum geometry. When the terrestrial parallactic angle is close to 60°, this combined with any aerial parallactic angle greater than 30° provides excellent geometry. A terrestrial parallactic angle close to 30° provides a very weak geometry and should be avoided. The role of the aerial photograph is very important as it increases the relative precision from 20% up to 50% (Table 2.9). A photogrammetric method for large structure monitoring, therefore, should, where feasible, include a combination of aerial and terrestrial photography.

3.0 MATHEMATICAL CONCEPT AND ADJUSTMENT

3.1 Definition of the Mathematical Model

The mathematical model as defined by Mikhail, 1976, is a theoretical system or an abstract concept by which one describes the physical situation of a set of events. For photogrammetry, the mathematical model is defined by the central projection, where object points are projected through two or more perspective centers and are imaged in two or more corresponding image planes (see also Argyris, 1972). The perspective center of the projection is the frontal nodal point of the lens of the taking camera, while the image plane on which the object points are imaged, is the photographic emulsion mounted on stable based material precisely located at the focal plane of the camera.

Figure 3.1 shows the mathematical model set up adopted for the present research. In this figure object points A, B and C are projected through the perspective centers O' and O", which are the frontal nodal points of the left and right exposure stations respectively. These points are imaged in the positive image planes E_1 and E_2 creating the images a', b', c' and a", b", c". The geometry of the mathematical model can be reconstructed either analogically or analytically.

Analogic processes are typically of lower precision as compared to the analytical approach. The analogical reconstruction of the imaging process will not be further considered in the following discussion. The analytical process can be carried out by employing various mathematical methods which are based on principles of projective or solid analytic geometry. The optimum condition, which is generally adopted to express mathematically the interrelation of the elements of the pho-

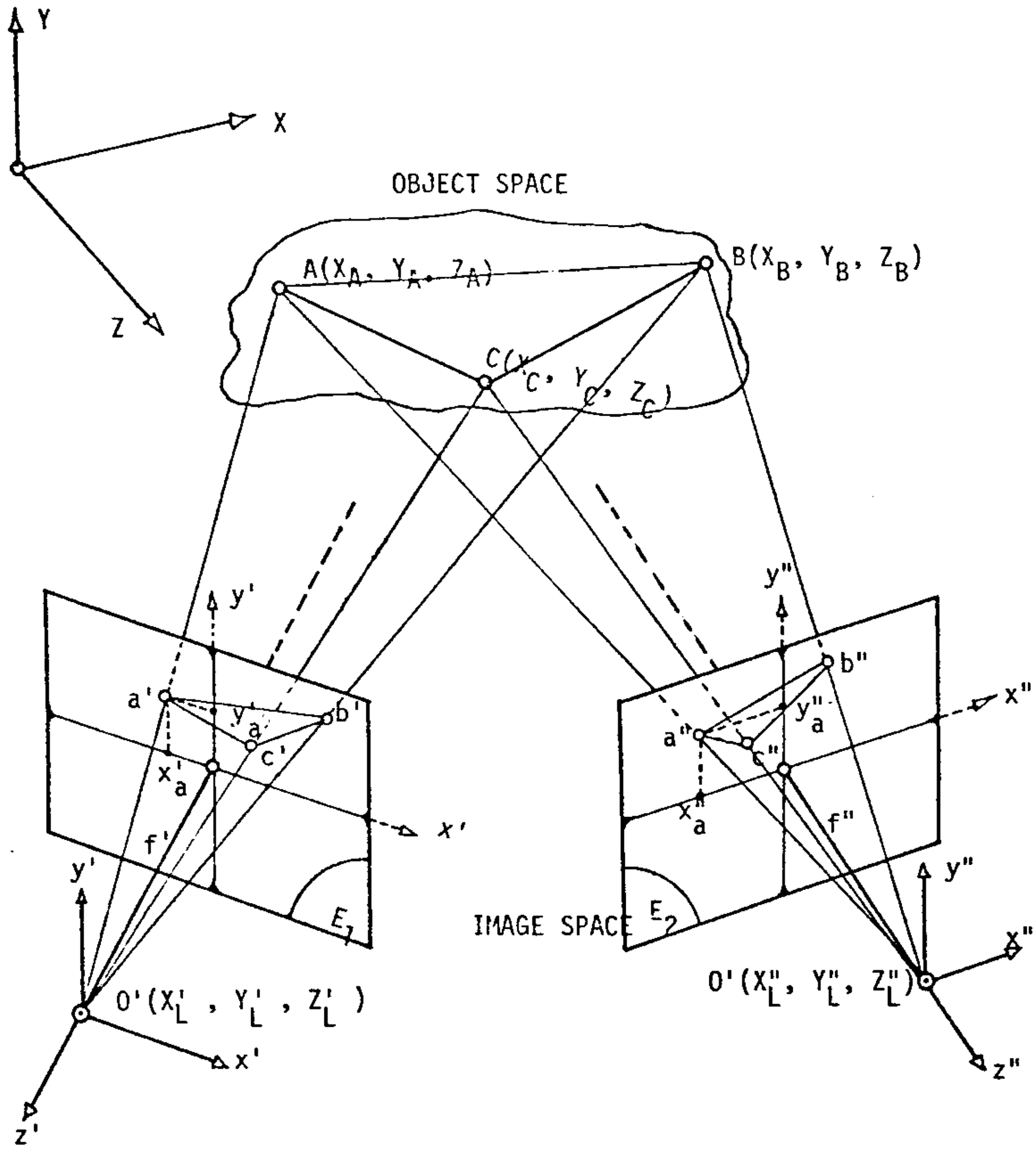

Fig. 3.1. The mathematical model in photogrammetry.

togrammetric model, is the collinearity condition. The basic principle in the collinearity condition, is that (ref. to Fig. 2.1) the object point A, its image a' and the frontal nodal point at the left exposure station O', lie along the same straight line. Similar conditions exist for any object point and any photograph on which that point is imaged. For the object point A and for its image a' in the left photograph, the collinearity condition is expressed by the following formulas

$$x'_a = -f' \left[\frac{m'_{11}(X_A-X'_L) + m'_{12}(Y_A-Y'_L) + m'_{13}(Z_A-Z'_L)}{m'_{31}(X_A-X'_L) + m'_{32}(Y_A-Y'_L) + m'_{33}(Z_A-Z'_L)}\right]$$

$$y'_a = -f' \left[\frac{m'_{21}(X_A-X'_L) + m'_{22}(Y_A-Y'_L) + m'_{23}(Z_A-Z'_L)}{m'_{31}(X_A-X'_L) + m'_{32}(Y_A-Y'_L) + m'_{33}(Z_A-Z'_L)}\right] \qquad 3.1$$

where:

x'_a, y'_a are photo-coordinates reduced to the principal point of the photograph;

f' is the focal length of the left camera;

X_A, Y_A, Z_A are ground coordinates of the object point A;

X'_L, Y'_L, Z'_L are ground coordinates of the perspective center O';

m'_{11}, $m'_{12} \ldots m'_{33}$ are the elements of the M-rotational matrix.

These nine transformation elements can be expressed as functions of three rotational angles. These three rotational angles, ω, ϕ, κ are sequentially performing rotations around the X, Y, and Z axes respectively.

The equations 3.1 can be written in a matrix form as follows:

$$x'_a = -f' \frac{M'_1 \, X_A}{M'_3 \, X_A}$$

$$y'_a = -f' \frac{M'_2 \, X_A}{M'_3 \, X_A} \qquad 3.2$$

where M'_1, M'_2, M'_3 are row vectors given as follows:

$$M'_1 = [m'_{11} \; m'_{12} \; m'_{13}]$$
$$M'_2 = [m'_{21} \; m'_{22} \; m'_{23}]$$
$$M'_3 = [m'_{31} \; m'_{32} \; m'_{33}]$$

The X_A is a column vector given by

$$X_A = \begin{bmatrix} X_A - X'_L \\ Y_A - Y'_L \\ Z_A - Z'_L \end{bmatrix}$$

By changing the notation, using i for the i^{th} photograph and j for the j^{th} point, the equations 3.2 can be written in a general form:

$$x_{ij} = -f_i \frac{M_{1i} \, X_{ij}}{M_{3i} \, X_{ij}}$$

$$y_{ij} = -f_i \frac{M_{2i} \, X_{ij}}{M_{3i} \, X_{ij}} \qquad 3.3$$

The equations 3.3 define analytically the mathematical model in photogrammetry. In order to study some important characteristics of applied photogrammetry, such as the most favorable geometry, the systematic error effect, the accidental error effect, etc., certain simulation techniques are utilized.

3.2 Simultaneous Adjustment

There are several approaches for using a simultaneous adjustment method in photogrammetry. Brown, 1958, 1966, 1976, developed the bundle method which is the simplest and most rigorous method based on the collinearity condition (Eq. 2.1). It is used for all purposes such as large triangulation blocks, close range phototriangulation, etc. Dorrer, 1971 used complex numbers for block adjustment. Dorrer and Ball, 1973 apply tensor analysis to the simultaneous adjustment. Erlandson and Veress, 1975 use the combined observation and condition method for monitoring of structures. In the present literature, however, there is a tendency towards the bundle method because of the simplicity: Bauer and Müller, 1972; Schut, 1974; Wong, 1975; Fraser, 1979b, Salmenperä; Anderson and Savolainen, 1974. Many of the authors in recent developments have tried to model, as precisely as possible, the instrumental imperfections in the camera lens and some deformations caused by the material used (film unflatness, film shrinkage) by carrying additional parameters in the bundle method. This process is customarily called "self-calibration" or "bundle adjustment with additional parameters". Because of the simplicity and general adoption of the standard bundle method, it has been adopted for use in the present research.

The history of developments in simultaneous phototriangulation adjustment has paralleled the development of high speed computer systems. When one is dealing with a simultaneous adjustment method, it is necessary to formulate the problem in such a way so as to optimize the required computer memory storage and to minimize the processing time.

3.3 Basic Principles of the Bundle Method.

The collinearity equations 3.1 can be written in a general linear form: (Brown, 1976, see also Appendix C)

$$V_{ij}+\dot{B}_{ij}\dot{\delta}_i+\ddot{B}_{ij}\ddot{\delta}_j = \varepsilon_{ij} \qquad 3.4$$

where: V_{ij} = 2 x 1 vector with corrections to the image coordinates

$\dot{B}_{ij}$ = 2 x 6 matrix of the partial derivatives of Eq. 3.1 with respect to the six orientation elements

$\dot{\delta}_i$ = 6 x 1 vector with corrections to the exterior orientation elements

$\ddot{B}_{ij}$ = 2 x 3 matrix of the partial derivatives of Eq. 3.1 with respect to the three coordinates of a ground point

$\ddot{\delta}_j$ = 3 x 1 vector with corrections to the three coordinates of a ground point

ε_{ij} = 2 x 1 vector with the differences between approximated values of Eq. 3.1 and observed values.

The subscript i refers to the number of the photograph and the j refers to the number of the measured point. The partial derivatives of equations 3.1 are evaluated using approximate values. By applying least-squares principles the normal equations are obtained as follows

$$\begin{bmatrix} \dot{N}+\dot{W} & \bar{N} \\ \bar{N}^T & \ddot{N}+\ddot{W} \end{bmatrix} \begin{bmatrix} \dot{\delta} \\ \ddot{\delta} \end{bmatrix} = \begin{bmatrix} \dot{c} - \dot{W}\dot{\varepsilon} \\ \ddot{c} - \ddot{W}\ddot{\varepsilon} \end{bmatrix} \qquad 3.5$$

where: $\dot{N} = \dot{B}^T W \dot{B}$

W = a diagonal matrix with the weights of the observed photo-coordinates

$\dot{W}$ = the inverse variance-covariance matrix of the a priori estimates of the camera exterior orientation elements (usually diagonal).

$\ddot{N} = \ddot{B}^T W \ddot{B}$

$\ddot{W}$ = the inverse variance-covariance matrix of the a priori ground coordinate estimates (usually diagonal).

$\bar{N} = \dot{B}^T W \ddot{B}$

$\dot{c} = \dot{B}^T W \varepsilon$

$\ddot{c} = \ddot{B}^T W \varepsilon$

$\dot{\varepsilon}$ = vector of discrepancies between a priori (or observed) values of elements of exterior orientation and corresponding values used in the linearization of Eq. 3.1.

$\ddot{\varepsilon}$ = vector of discrepancies between a priori (or observed) values of coordinates of measured object points and corresponding values used in linearization of Eq. 3.1

A direct solution of equations 3.6 gives the corrections $\dot{\delta}$ and $\ddot{\delta}$ which subsequently are added to the corresponding approximate values. The problem solution is carried out by iterations. In the last iteration the corrections $\dot{\delta}$ and $\ddot{\delta}$ will approach zero in value.

As reported by Brown, 1976, the normal equations can be derived directly from the observation equations without the need for any intermediate operations. This analysis is based on the fact that the normal equations are composed of submatrices as follows:

$$\left[\begin{array}{ccc|ccc} \dot{N}_1+\dot{W}_1 & 0\ldots & 0 & \bar{N}_{11} & \bar{N}_{12}\ldots & \bar{N}_{1m} \\ 0 & \dot{N}_2+\dot{W}_2\ldots & 0 & \bar{N}_{21} & \bar{N}_{21}\ldots & \bar{N}_{1m} \\ \vdots & \vdots & \vdots & \vdots & \vdots & \vdots \\ 0 & 0\ldots & \dot{N}_m+\dot{W}_m & \bar{N}_{m1} & \bar{N}_{m2}\ldots & \bar{N}_{mm} \\ \hline \bar{N}^T_{11} & \bar{N}^T_{21}\ldots & \bar{N}^T_{m1} & \ddot{N}_1+\ddot{W}_1 & 0\ldots & 0 \\ \bar{N}^T_{12} & \bar{N}^T_{22}\ldots & \bar{N}^T_{m2} & 0 & \ddot{N}_2+\ddot{W}_2\ldots & 0 \\ \vdots & \vdots & \vdots & \vdots & \vdots & \vdots \\ \bar{N}^T_{1m} & \bar{N}^T_{2m}\ldots & \bar{N}^T_{mm} & 0 & 0\ldots & \ddot{N}_n+\ddot{W}_n \end{array}\right] \left[\begin{array}{c} \dot{\delta}_1 \\ \dot{\delta}_2 \\ \vdots \\ \dot{\delta}_m \\ \hline \ddot{\delta}_1 \\ \ddot{\delta}_2 \\ \vdots \\ \ddot{\delta}_n \end{array}\right] = \left[\begin{array}{c} \dot{c}_1-\dot{W}_1\dot{\varepsilon}_1 \\ \dot{c}_2-\dot{W}_2\dot{\varepsilon}_2 \\ \vdots \\ \dot{c}_m-\dot{W}_m\dot{\varepsilon}_m \\ \hline \ddot{c}_1-\ddot{W}_1\ddot{\varepsilon}_1 \\ \ddot{c}_2-\ddot{W}_2\ddot{\varepsilon}_2 \\ \vdots \\ \ddot{c}_n-\ddot{W}_n\ddot{\varepsilon}_n \end{array}\right] \qquad 3.6$$

Each submatrix comprises values which are accumulated directly from the observation equations. According to Brown, 1976, with reference to the observation equations corresponding to the i^{th} photograph and j^{th} point (Eq. 3.4), the following submatrices can be directly formed:

$$\dot{N}_{ij} = \dot{B}^T_{ij}\ W_{ij}\ \dot{B}_{ij}$$

$$\bar{N}_{ij} = \dot{B}^T_{ij}\ W_{ij}\ \ddot{B}_{ij}$$

$$\ddot{N}_{ij} = \ddot{B}^T_{ij}\ W_{ij}\ \ddot{B}_{ij}$$

$$\dot{c}_{ij} = \dot{B}^T_{ij}\ W_{ij}\ \varepsilon_{ij}$$

$$\ddot{c}_{ij} = \ddot{B}^T_{ij}\ W_{ij}\ \varepsilon_{ij} \qquad 3.7$$

Then the normal equations are obtained by accumulation as follows:

$$\dot{N}_i = \sum_{j=1}^{n} \dot{N}_{ij} \qquad \dot{c}_i = \sum_{j=1}^{n} \dot{c}_{ij}$$

$$\ddot{N}_j = \sum_{i=1}^{m} \ddot{N}_{ij} \qquad \ddot{N}_j = \sum_{i=1}^{m} \ddot{c}_{ij} \qquad 3.8$$

In the present research the normal equations are based on Brown's concept but they are obtained in a slightly different way which is given in detail in the following section.

3.4 Organization of the Simultaneous Adjustment.

Applications of the bundle method have been reported for aerial triangulation, as well as for close range photogrammetry. Photogrammetry for large structural monitoring is, however, a special case of non-topographic photogrammetry and the bundle method is employed in this field to rigorously optimize the designed photogrammetric survey system. The optimization is dependent on the way to form and solve the normal equations. For the present experimental monitoring the number of camera stations is relatively few. A practical maximum of six camera stations are able to cover all sides of the large structure assuming that two of them will be aerial photographs. The use of six camera stations has also been reported by Brandenberger and Erez, 1972. The number of points to be monitored is relatively large compared to the number of camera stations. One hundred points are sufficient to cover the present structure (Veress, Jackson and Hatzopoulos, 1979). In writing the computer program, provisions have been made for the inclusion of six cameras and one hundred points in the bundle adjustment. The maximum size of the normal equation coefficient matrix will then be: $n = 36$, $m = 300$; $(n + m) \times (n + m) = 112896$ ($\approx$ 334400 octal). The requirement of such core storage for one matrix is neither economical nor practical. However, the system can be greatly economized by storing the normal equation submatrices separately in symmetric storage mode and ignoring null submatrices of $\dot{N} + \dot{W}$ and $\ddot{N} + \ddot{W}$. In this case $\dot{N} + \dot{W}$ will have 126 non-zero elements or $6\times[6\times(6+1)/2]$. The submatrix $\ddot{N} + \ddot{W}$ will have 600 non-zero elements $(100 \times [3 \times (3 + 1)/2])$ and the submatrix $\bar{N}^T$ will have: 10800 elements including zeros (36×300). In this way the maximum elements of the normal equations in symmetric storage mode will be 11,526 or 26.4K. Since the number of camera stations and the number of ground points is known the normal equation submatrices can be initialized by zeros. At the same time the order of the photographs and the order of the ground points within the normal equations is set up, following the derivation of the observation equations for one image point at a time. This is performed by a subroutine. The linear form of the observation equations for one image point can then be written as:

$$V_x + (a_1 \quad a_2 \quad a_3 \quad a_4 \quad a_5 \quad a_6)\dot{\delta}_i + (a_7 \quad a_8 \quad a_9)\ddot{\delta}_j = a_{10}$$

$$V_y + (b_1 \quad b_2 \quad b_3 \quad b_4 \quad b_5 \quad b_6)\dot{\delta}_i + (b_7 \quad b_8 \quad b_9)\ddot{\delta}_j = b_{10} \qquad 3.9$$

The equations 3.9 are similar to the equations 3.4 and they are related as follows:

$$V_{ij} = \begin{bmatrix} V_x \\ V_y \end{bmatrix}$$

$$B_{ij} = \begin{bmatrix} a_1 & a_2 & a_3 & a_4 & a_5 & a_6 \\ b_1 & b_2 & b_3 & b_4 & b_5 & b_5 \end{bmatrix}$$

$$B_{ij} = \begin{bmatrix} a_7 & a_8 & a_9 \\ b_7 & b_8 & b_9 \end{bmatrix}$$

$$\varepsilon_{ij} = \begin{bmatrix} a_{10} \\ b_{10} \end{bmatrix}$$

(See Appendix A for detailed evaluation of a_K and b_K, K=1,10)

Each equation of the 3.9 is divided by the standard error of the particular observation (3μm for instance) and then the coefficients a_K (K=1, 10) are multiplied in pairs, i.e. a_1a_1, a_1a_2, a_2a_2, a_2a_3....(see Fig. 3.2) finally 54 individual products are created. The product $a_{10}a_{10}$ is not used. These products are organized as shown in Fig. 3.2. For the i^{th} photograph and the j^{th} ground point, the values from group I (Fig. 3.2) are added to the $\dot{N}_i$ submatrix of Eq. 3.9, the values from group II are added to the $\overline{N}_{ij}$, the values from group III are added to $\ddot{N}_j$, the values from group IV form the $\dot{c}_i$ and finally the values from group V form the $\ddot{c}_j$. The same procedure can be followed by using the b_K (K=1, 10) coefficients of Eq. 3.9. With this technique the normal equations are obtained by using one observation equation at a time. The image coordinates can also be in any order; no special arrangement is necessary.

Fig. 3.2 indicates the structural cells of the normal equation submatrices. The groups I and III in Fig. 3.2 are presented in a lower triangular symmetric storage mode. The solution of the normal equations is performed by partitioning the coefficient matrix in the position shown in Eq. 3.6 by dashed lines.

I — 21 elements of $\dot{N}_i$

a_1a_1					
a_1a_2	a_2a_2				
a_1a_3	a_2a_3	a_3a_3			
a_1a_4	a_2a_4	a_3a_4	a_4a_4		
a_1a_5	a_2a_5	a_3a_5	a_4a_5	a_5a_5	
a_1a_6	a_2a_6	a_3a_6	a_4a_6	a_5a_6	a_6a_6

II — 18 elements of $\bar{N}_{ij}$

a_1a_7	a_2a_7	a_3a_7	a_4a_7	a_5a_7	a_6a_7
a_1a_8	a_2a_8	a_3a_8	a_4a_8	a_5a_8	a_6a_8
a_1a_9	a_2a_9	a_3a_9	a_4a_9	a_5a_9	a_6a_9

III — 6 elements of $\ddot{N}_j$

a_7a_7		
a_7a_8	a_8a_8	
a_7a_9	a_8a_9	a_9a_9

IV — 6 elements of $\dot{c}_i$

a_1a_{10}	a_2a_{10}	a_3a_{10}	a_4a_{10}	a_5a_{10}	a_6a_{10}

V — 3 elements of $\ddot{c}_j$

a_7a_{10}	a_8a_{10}	a_9a_{10}

Fig. 3.2 Organization of normalized values obtained from an observation equation of the x-coordinate. These values are ready to be directly accumulated into the initialized locations of the normal equations.

First the $\ddot{N} + \ddot{W}$ matrix is inverted. This matrix is formed from 3 x 3 block diagonal submatrices which are inverted one at a time. Two new matrices then are generated as follows: (Brown, 1976).

$$G = -(\ddot{N} + \ddot{W})^{-1}\overline{N}^{T}$$

$$D = (\dot{N} + \dot{W}) + \overline{N}G \qquad 3.10$$

The size of the D matrix is strictly dependent on the number of camera stations, by using six camera stations the order of the D matrix is 36 x 36. The matrix D is stored in a symmetric storage mode. The D matrix is substituted by the D^{-1} which is obtained by using Cholesky's matrix invertion method (Bjerhammar, 1973).

The elements of the vectors $\dot{\delta}$ and $\ddot{\delta}$ are computed as follows:

$$\dot{\delta} = D^{-1}[G^{T}(\ddot{c}-\ddot{W}\ddot{\varepsilon}) + \dot{c}-\dot{W}\dot{\varepsilon}]$$

$$\ddot{\delta} = (\ddot{N}+\ddot{W})^{-1}(\ddot{c}-\ddot{W}\ddot{\varepsilon}) + GD^{-1}[G^{T}(\ddot{c}-\ddot{W}\ddot{\varepsilon}) + \dot{c} + \dot{W}\dot{\varepsilon}] \qquad 3.11$$

The variance-covariance matrix of the exterior orientation parameters is given as: $Q_{LL} = D^{-1}$. The variance-covariance matrix of the ground points is given by:

$$Q_{XX} = (\ddot{N}+\ddot{W}) + GD^{-1}G^{T} \qquad 3.12$$

The matrix $GD^{-1}G^{T}$ is evaluated in steps one row at a time, the row then being added to the corresponding row of the $(\ddot{N}+\ddot{W})$ matrix.

The last iteration is determined by checking a maximum angular correction to the exterior orientation elements of 10^{-5} radians. After the last iteration occurs, the V_{ij} values are computed from Eq. 3.4.

The standard error of the unit weight is computed as follows (assuming $\dot{\delta} \approx 0$, $\ddot{\delta} \approx 0$):

$$\sigma_0^2 = \frac{V^T W V + \dot{\varepsilon}^T \dot{W} \dot{\varepsilon} + \ddot{\varepsilon}^T \ddot{W} \ddot{\varepsilon}}{DF} \qquad 3.13$$

Where DF are the degrees of freedom, the degrees of freedom usually are equal to the number of the observation equations plus the number of fixed parameters. A minimum of seven fixed parameters is required to have a definite solution from the normal equations. The standard errors then are obtained as:

$$\sigma_{\dot{\delta}}^2 = \sigma_\delta^2 q_{LL}$$
$$\sigma_{\ddot{\delta}}^2 = \sigma_\delta^2 q_{XX} \qquad 3.14$$

Where $\sigma_{\dot{\delta}}$ is the standard error for an exterior orientation parameter,

$\sigma_{\ddot{\delta}}$ is the standard error for a ground point parameter.

q_{LL} is a diagonal element of the Q_{LL} matrix.

q_{XX} is a diagonal element of the Q_{XX} matrix.

The computer program which has been developed for the simultaneous method is named PHOMO and is based on the foregoing formulation of the problem. Any number of photographs or points can be accommodated by changing appropriate dimension statements in the various programs. In this way, by using fifty points, six camera stations and two hundred images, a central memory of 54.7K of the University of Washington CDC 6400 system is required for the execution of program PHOMO. By using one hundred points, three camera stations and three hundred images a central memory of 61.4K is required. The computation time has a minimum value when only the unknown parameters are determined. The computation time increases rapidly when the variances and covariances of the unknown parameters are computed. Example: Using thirty-eight ground points, one hundred-eight images and five camera stations;

a) the computation time for determining the unknown parameters was only 13 seconds,

b) the computation time for determining the unknown parameters and their standard errors was 19 seconds,

c) the computation time for determining the unknown parameters and their variances-covariances was 33 seconds.

These variations in the computation time are created by the tremendous amount of computations involved in Equation 3.12 and it depends on which elements of the matrix $GD^{-1}G^{T}$ (see Eq. 3.12) are determined. Fig. 3.3 gives the organization of the Program PHOMO.

3.5 Sequential Adjustment

This adjustment method is performed in several sequential steps according to a certain order. The sequential steps are:

a. Reduction of the plate coordinates.

In this step the equations 4.1 are used for the camera which operates glass plates. Then the autocollimation point correction is performed and finally the lens distortion is compensated for by using formulas 4.5. Finally, appropriate corrections for refraction are performed by formulas 4.7.

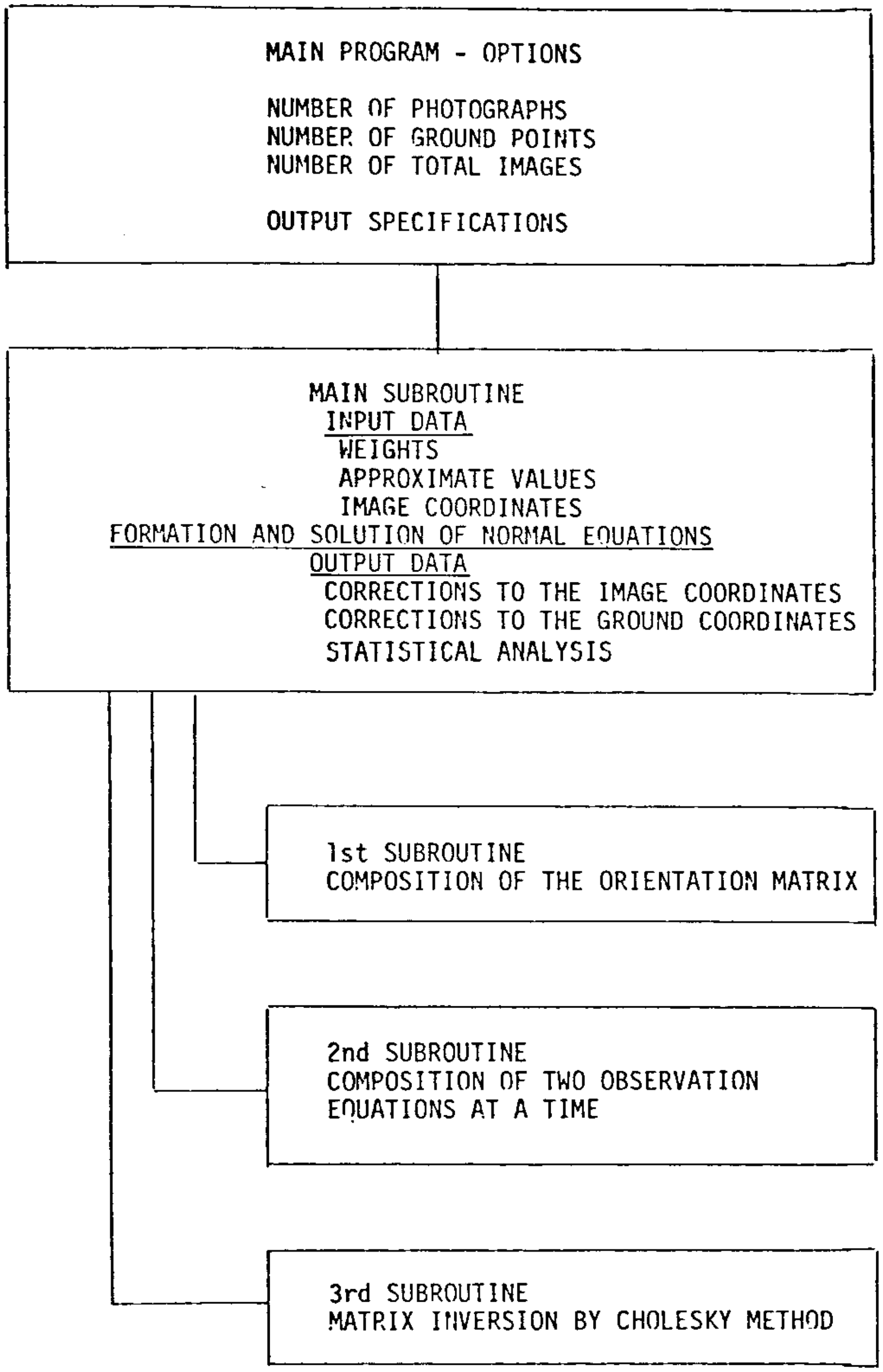

Fig. 3.3 Organization of the simultaneous bundle adjustment computer program PHOMO.

b. Space resection.

The frontal nodal point of the camera station is determined by assigning approximate coordinates to it and computing a resection using the image and ground coordinates of a minimum of three control points. The method is based on vector analysis as given by Erlandson and Veress, 1975. Another method for space resection is based on the collinearity condition. In this method the frontal nodal point of the camera station as well as the rotation angles ω, ϕ, κ can be simultaneously computed. This method is usually used for the aerial camera.

c. Orientation matrix.

The rotational matrix is determined as follows: The image coordinates are related to the ground coordinates through the following equation:

$$\begin{bmatrix} x \\ y \\ -f \end{bmatrix} = M \begin{bmatrix} X - X_L \\ Y - Y_L \\ Z - Z_L \end{bmatrix} \qquad 3.15$$

where: x, y are refined image coordinates,

f is the camera focal length,

X, Y, Z are ground coordinates of a control point,

X_L, Y_L, Z_L are the frontal nodal point coordinates of the camera station,

M is the rotational matrix to be determined.

A minimum of three control points are required to directly compute the nine elements of the rotational matrix M (Ghosh, 1975).

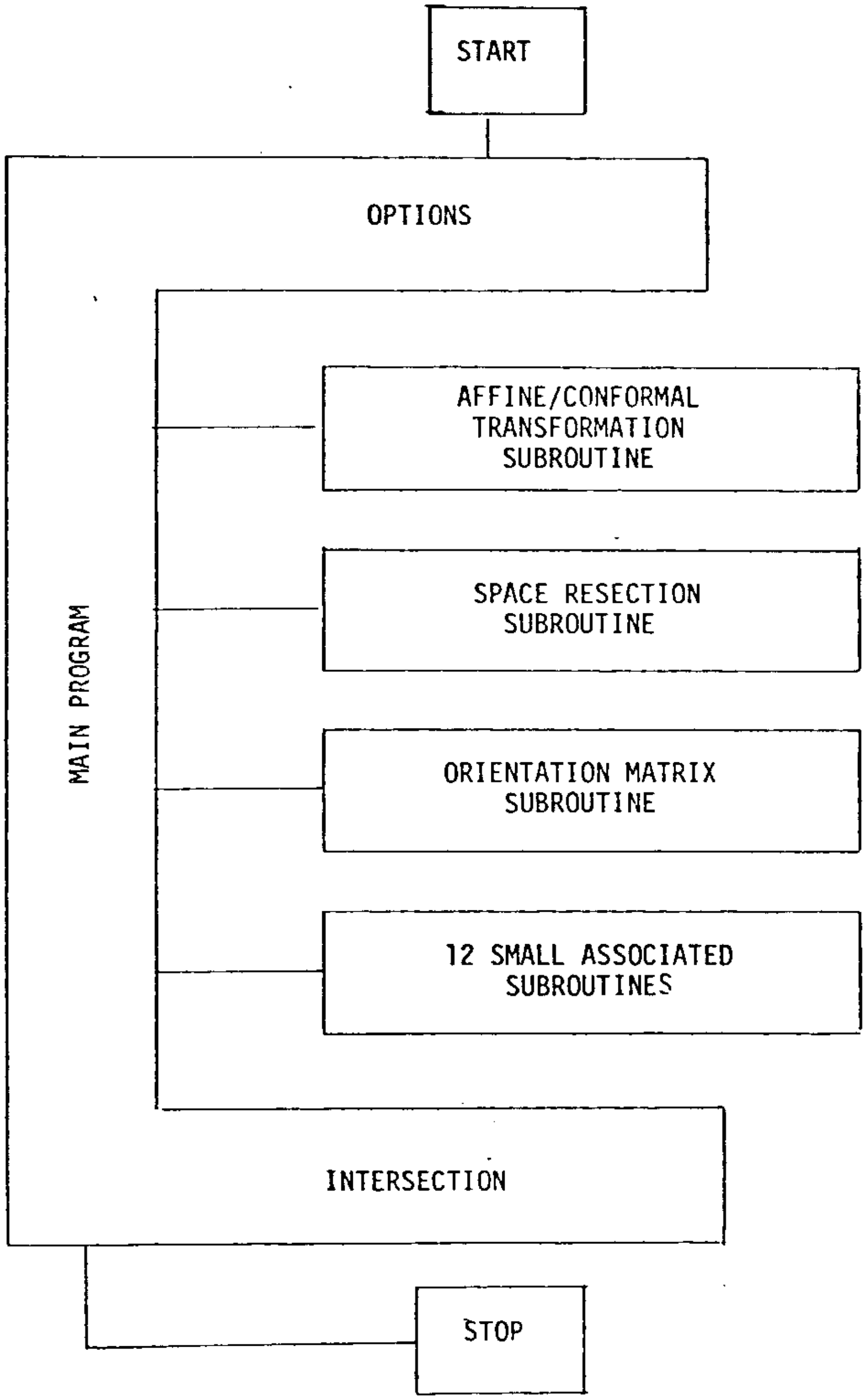

Fig. 3.4. Organization of the basic subroutines.

d. Space intersection.

The intersection of two or more light rays, which correspond to the same object point imaged in two or more photographs, can be obtained mathematically by the collinearity condition (A.S.P. Manual, 1966; Wolf, 1974) or the vector method (Erlandson and Veress, 1975; Ball, 1973). There is no important difference by using either method. In the present research the vector method is used.

The sequential adjustment method is carried out by a computer program named SEQGE. The basic subroutines of SEQGE are illustrated in Figure 3.4 while the data organization is illustrated in Figure 3.5. The program is flexible, providing many options.

The main segment of the program is able to run with or without calling the basic subroutines and with or without intersection. It is possible, for instance, to compute only the affine transformation coefficients and print or punch the results without running any other subroutine or without performing intersection. The program can handle up to five camera stations and up to twenty control points. It performs intersection with two or more camera stations. The input data is controlled by an options card which specifies what subroutines are going to be used, what input parameters should be expected and if punched output is desired.

The output provides a list of the input data for checking purposes and also provides a list of the refined image coordinates. The orientation matrix is always printed in the output, either in matrix form with nine elements or in rotation angle form as ω, ϕ, κ in degrees, minutes and seconds.

Finally there is a list of X, Y, Z ground coordinates of the intersected points with their associated standard errors and variance-covariance matrices. The program SEQGE is capable of providing most of the necessary data which subsequently can be used in a computer program based on a simultaneous adjustment.

In the case of using film instead of glass plates, such as an aerial film camera, another computer program named CARVL performs the initial image coordinate reduction using formulas 4.1. The output of this program can be used either for the program SEQGE or for a simultaneous adjustment. For the aerial photograph a special resection computer program has been developed. It is named RESAE and it is based on the collinearity condition. The input data is approximate coordinates of the exterior orientation parameters and a minimum of three control points. The output data is the exterior orientation parameters. This program has already been submitted to the Washington State Department of Transportation and is now in operation.

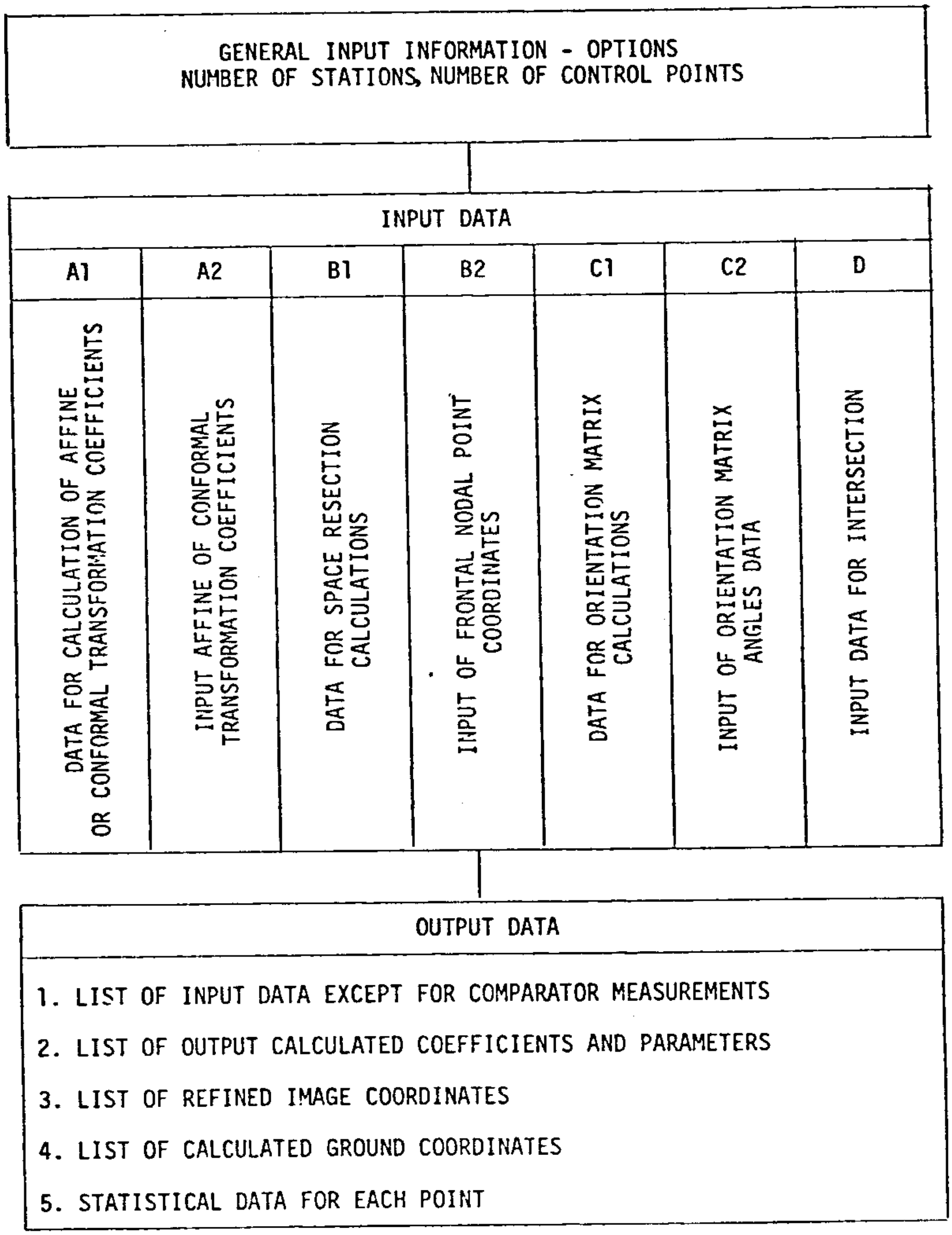

Fig. 3.5. Data organization

4.0 DATA ACQUISITION AND REFINEMENT

4.1 Data Acquisition

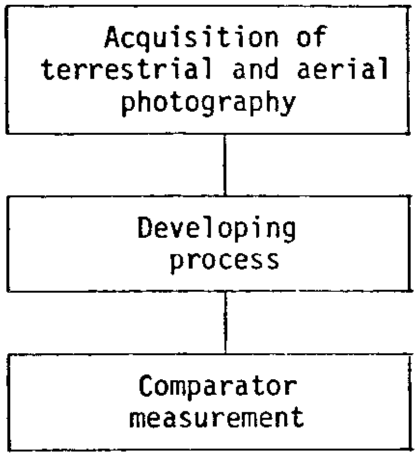

Fig. 4.1 Flow chart diagram for data acquisition.

The data acquisition is shown in Fig. 4.1 as a flow chart diagram. There are three phases. The first phase involves taking the actual photographs. This phase should be given special attention particularly the exposure of the first set of photographs which will be the basis of comparisons for all the subsequent sets. The terrestrial and aerial photographs must be obtained within a half an hour to one hour time interval. In this way a minimal differential motion of the structure will take place. For prolonged measurements, temperature and other factors may cause differential movements in the structure which do not appear on all exposures.

The second phase is the darkroom process which involves developing the plates or the films. When there is more than one exposed plate from the same exposure station, the first plate is developed in a regular developing time. Then if there is any problem, the developing time is adjusted so as to obtain a desirable image quality for each subsequent plate. It is helpful to develop paper prints of the first set of photographic negatives and to mark on these photographs all control points and target points to be measured on the structure. This facilitates theeasy identification of targets in any set of photographs. After the darkroom process, the third phase or the comparator measurement takes place. The photographic x, y coordinates are measured starting with the fiducial marks then the control points and finally all other target points. It is recommended that four measurements be made at each fiducial mark and control point and at least two coordinate measurements of each of the other image points.

After the observations are completed, the observed values must be averaged and their standard errors must be recorded. According to the specifications given by Erlandson and Veress, 1975 for monitoring application when the standard error of an observed value is greater than 6μm, this value must be rejected.

At this point the data obtained are ready for refinement. The subsequent reduction computations will be discussed in the following sections.

4.2 Coordinate Reduction and Correction for Film Distortion

Corrections for film distortion and comparator errors, as well as image coordinate transformation for the comparator system to the image system, can all be achieved to a large degree by using the bilinear equations.

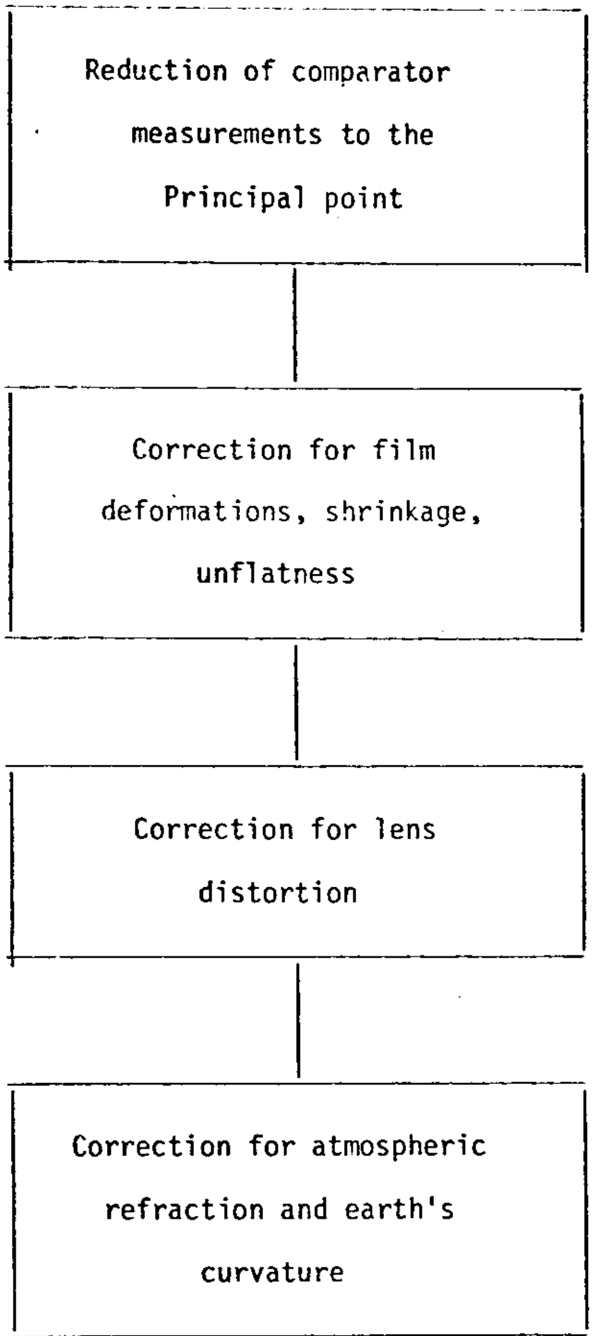

Fig. 4.2 Flow chart diagram for data refinement.

$$x' = x + a_1 + b_1x + c_1y + d_1xy$$
$$y' = y + a_2 + b_2x + c_2y + d_2xy \qquad 4.1$$

Where x', y' are the corrected coordinates of photopoints;

x, y are the observed (uncorrected) coordinate values;

a_1, b_1,...d_2 are the coefficients to be determined.

The four fiducial marks yield four sets of such equations and provide a unique determination for the coefficients a_1, b_1...d_2. The individual terms of Eq. 4.1 make corrections for several influences at the same time.

1. a_1 and a_2 provide translations to the origin from the comparator system to the principal point of the photographs.
2. b_1, b_2, c_1, c_2
   a. Accomplish the rotation of the observed system
   b. Account for the nonperpendicularity of the comparator axes.
   c. Correct the skewness of axes caused by film distortion
   d. Correct the scale differences in x and y regardless of whether the error is caused by differential film distortion or errors in the comparator
3. d_1 and d_2 provide a quadratic or curvilinear correction for film distortion.

Equation 4.1 can, therefore, be used to compensate for much of the film deformation. When glass plates are used, the d_1 and d_2 coefficients can be neglected and an affine transformation can be carried out as follows:

$$x' = x + a_1 + b_1 x + c_1 y$$
$$y' = y + a_2 + b_2 x + c_2 y \qquad 4.2$$

Finally, if necessary, the image coordinates should be reduced to the autocollimation point of the photo as follows:

$$x'' = x' - x_o$$

$$y'' = y' - y_o$$

Where x", y" are the reduced coordinates

x_o, y_o are the autocollimation point coordinates.

4.3 Correction for Lens Distortion

Generally, the most significant distortion caused by the camera lens is the symmetric radial lens distortion. In Fig. 4.3 the point a is the correct image location of an object point. Due to the radial lens distortion, the point a is displaced to the position a'. The displacement is positive when radially outward from the principal point of the photograph. The displacement Δr can be expressed as a function of the radial distance r which is the distance between the image point a and the principal point of the photo.

$$\Delta r = K_1 r + K_2 r^3 + K_3 r^5 + \ldots \qquad 4.3$$

Where K_1, K_2, K_3 are coefficients which are determined from the camera calibration data. The corrections to be given to the image coordinates are as follows:

$$\frac{\Delta r}{r} = \frac{\Delta x}{x} = \frac{\Delta y}{y} \qquad 4.4$$

and

$$\Delta x = \frac{x}{r}\,\Delta r \qquad \Delta y = \frac{y}{r}\,\Delta r$$

or combining Equations 4.3 and 4.4

$$\Delta x = x(K_1 + K_2 r^2 + K_3 r^4)$$

$$\Delta y = y(K_1 + K_2 r^2 + K_3 r^4) \qquad 4.5$$

Where $r = \sqrt{x^2 + y^2}$

The coefficients used in Equations 4.5 give satisfactory results, whereas adding more coefficients corresponding to a higher order r often does not lead to any significant improvements, especially for simple lenses.

The corrected coordinates will be:

$$x' = x - \Delta x = x(1 - K_1 - K_2 r^2 - K_3 r^4)$$

$$y' = y - \Delta y = y(1 - K_1 - K_2 r^2 - K_3 r^4) \qquad 4.6$$

The decentering distortion has a smaller effect in the image coordinates. In a monitoring project where the camera stations are located in specific places, not necessarily fixed, the optics have a constant systematic effect which does not influence the relative structural motion measurements. It is hard, however, to establish a specific location of the aerial platform, but it is possible to approximate a near permanent aerial station by using the same aeroplane, same pilot, approximately the same flight lines, and exposing many frames. Then the frame which provides specified image scale and proper view of the structure would be considered as taken from an approximately permanent aerial platform.

4.4 Earth's Curvature and Atmospheric Refraction

By using a horizontal plane tangent to one of the base line stations as a datum, the earth's curvature effect is eliminated. The atmospheric refraction always influences the imaging process, to an extent, dependent on the meteorological conditions which exist at the moment of the exposure. As is stated by Fraser, 1979a: at a range of 1km the apparent object point position can be in error by as much as 2-3cm in normal meteorological conditions when using terrestrial cameras with 24" focal length. For the aerial photograph, the refraction in terms of image coordinates is about 1μm when the altitude is about 1,000 feet and the focal length of the camera is 6" (A.S.P. Manual, 1966). In the monitoring, however, the refraction is significant only for the terrestrial photography and when using large focal length. The problem can be solved using several methods given by Fraser, 1979a. Two of these methods are given as follows:

a. Corrections to the image coordinates by using the formulas (ref. to Fig. 4.4):

$$\Delta x = -f \sec^2(\beta-\omega)\Delta\beta \sin k$$
$$\Delta y = -f \sec^2(\beta-\omega)\Delta\beta \cos k \qquad 4.7$$

where $\Delta\beta$ is defined as $\Delta\beta = -\frac{S}{2} \cos \beta(\frac{dN}{dh}) \times 10^{-6}$

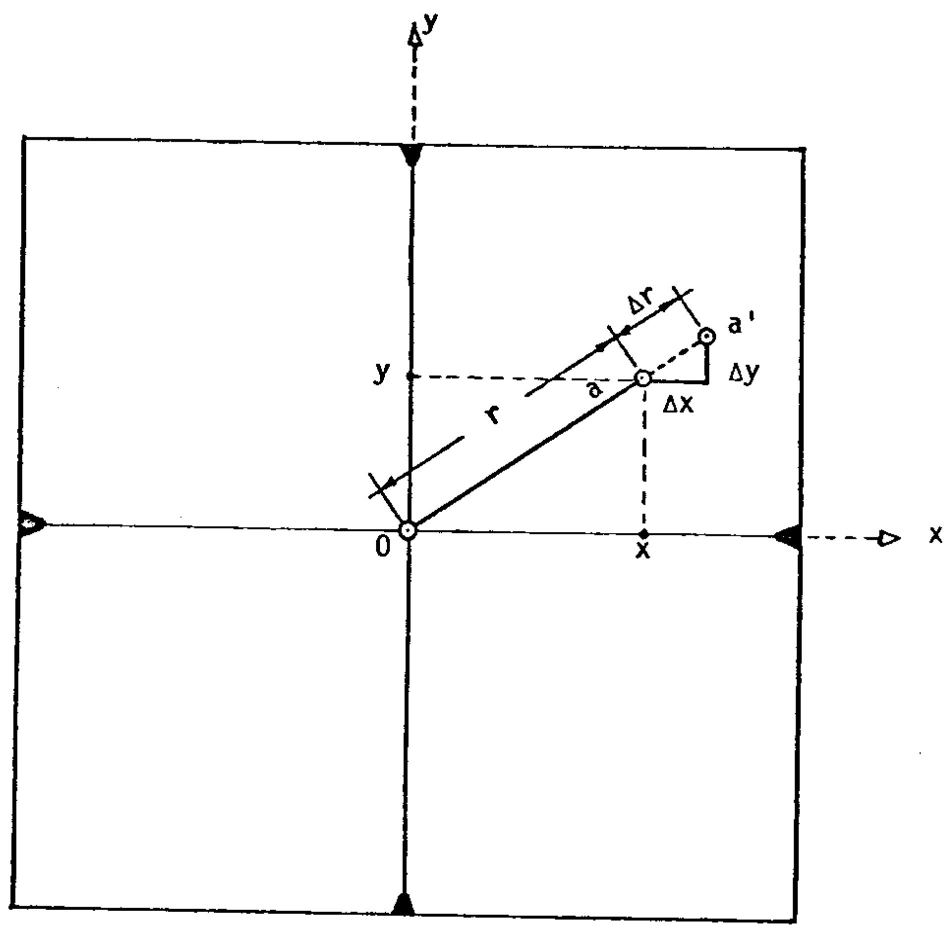

Figure 4.3. Radial lens distortion.

where $\frac{dN}{dh}$ is the vertical gradient of refractivity which is assumed to be constant along the light ray path. The $\frac{dN}{dh}$ can be evaluated from an estimate of the vertical temperature profile.

b. The effect of the vertical refraction in the object point coordinates can be reduced to a few micrometres over a photographic distance of one kilometre. This reduction is done by applying a priori constraints to the object control points and employing an analytical solution where the exterior orientation elements are treated as unknowns.

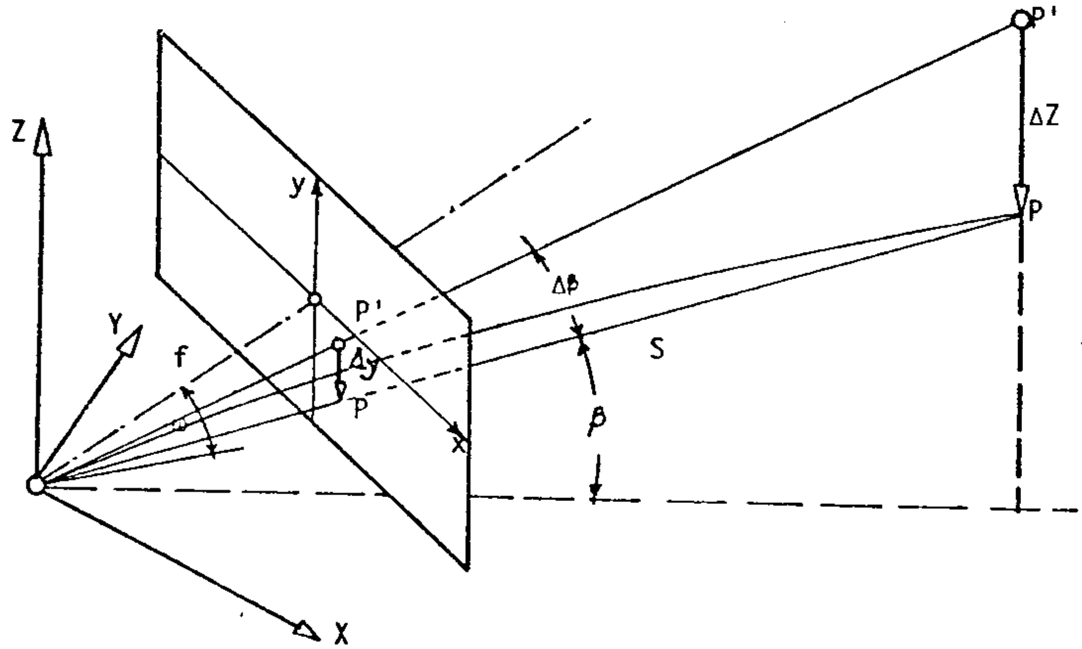

Fig. 4.4. Image coordinate correction ΔY and space coordinate correction ΔZ for vertical refraction (after Fraser, 1979).

5.0 THEORETICAL EVALUATION

5.1 Theoretical Evaluation Process

The theoretical evaluation is performed in order to establish that the methods developed, sequential and simultaneous, perform properly. Parallel to this, theoretical data adjusted using both methods are analyzed and compared. In the process of the theoretical evaluation, the effect of various errors, which are introduced to the image coordinates, is analyzed. The theoretical evaluation is based on a simulation experiment using data as in section 2.1. The parallactic angles and the exterior orientation elements are given in Table 5.1. In this experiment, only one combination is used as shown in Table 5.1. A total of sixteen experimental runs are performed.

Table 5.1 Parameters used for theoretical evaluations

Station No.	X_L	Y_L	Z_L	ω	ϕ	κ	Parallactic angle
1	-1500	1440	4300	0°	-30°	0°	P_t = 60°
2	5500	1460	4301	0°	30°	0°	
3	2015	2600	-400	-40°	0°	0°	P_a = 40°

Eight of these runs are performed by the sequential adjustment computer program plus eight by the simultaneous adjustment program. The various perturbations which are introduced to the image coordinates are as follows: Round-off errors to the closest micrometre. Autocollimation point error up to 20μm. Lens distortion error generated by the average distortion coefficients listed in Table 2.3. Accicental error as given in Table 2.4. Table 5.2 gives the final results obtained by the simulation experiment. The quantities S_X, S_y, S_Z of this table represent the mean square value of the differences as defined in Section 2.1. The quantity S_p is the position error defined as

$$S_p = \sqrt{S_X^2 + S_Y^2 + S_Z^2}$$

For all sequential runs, the exterior orientation elements are computed using perturbed image coordinates. For the simultaneous method the a priori variances given to the observed or estimated quantities are as follows: Frontal nodal point space coordinates; ±2 feet, orientation angles; ±180 minutes, observed image coordinates ±3μm, estimated or observed ground coordinates ±0.5 feet. The final differences between the true values of the exterior orientation elements as given by Table 5.1 and those values obtained by computation of the simulation experiment, are given by Tables 5.3 and 5.4.

5.2 Analysis of Results

The results presented by Table 5.2 provide a basis for the evaluation of the simulation experiment. Both adjustment methods are compared using the results given by Tables 5.2, 5.3 and 5.4. The most important difference between the two methods is found to be the effect of the autocollimation point error. In this case, the sequential method provides substantially larger differences from the true values whereas the simultaneous method provides smaller differences (about nine times better results from the sequential method). The autocollimation point error in the simultaneous adjustment is absorbed uniformly by the ex-

Table 5.2. Theoretical evaluation results

Errors in 1/1000 of a Foot

INTRODUCED ERROR SOURCE	SEQUENTIAL				SIMULTANEOUS				REMARKS
	s_X	s_Y	s_Z	s_P	s_X	s_Y	s_Z	s_P	
0	7.0	4.3	7.9	11.4	2.7	2.8	3.6	5.3	ROUND OFF ERROR
1	187.3	119.0	297.7	371.3	39.1	9.6	5.7	40.7	AUTOCOLLIMATION ERROR
2	24.7	14.3	41.4	50.3	18.1	13.9	32.1	39.4	LENS DISTORTION ERROR
3	197.1	127.4	304.3	384.3	38.6	9.5	31.7	50.8	AUTOCOLLIMATION LENS DISTORTION
4	44.2	33.7	56.4	79.2	49.9	28.5	52.1	77.6	ACCIDENTAL ERROR
5	218.7	120.5	317.1	403.6	47.8	29.1	53.2	77.2	ACCIDENTAL AUTOCOLLIMATION
6	49.7	35.2	66.3	90.0	48.6	34.9	61.8	86.0	ACCIDENTAL LENS DISTORTION
7	227.1	128.4	322.8	415.0	42.4	32.6	62.4	82.2	ACCIDENTAL AUTOCOLLIMATION LENS DISTORTION

Max autocollimation error introduced ≈ 20μm

Max lens distortion error introduced ≈ 16μm

Max accidental error introduced ≈ 6μm

Table 5.3. Changes of the exterior orientation elements computed by the sequential method

Station No.	Error source	1/1000 Feet			Minutes		
		ΔX_L	ΔY_L	ΔZ_L	$\Delta\omega$	$\Delta\phi$	$\Delta\kappa$
1	0	1	24	-25	0.01	-0.01	-0.02
	1	35	6	-31	0.13	0.11	0.05
	2	235	220	247	-0.13	-0.03	-0.09
	3	-202	203	241	0.01	0.08	-0.02
	4	441	-601	245	0.34	0.25	0.20
	5	475	-618	239	0.47	0.37	0.26
	6	205	-404	516	0.22	0.22	0.12
	7	239	-421	511	0.36	0.34	0.19
2	0	-25	-22	-30	0.01	-0.02	0.01
	1	-34	-21	39	0.14	0.08	-0.06
	2	59	132	281	-0.07	-0.05	0.07
	3	50	133	291	0.06	0.05	0.01
	4	84	409	-70	-0.24	0.08	0.03
	5	75	410	-60	-0.11	0.17	-0.04
	6	168	563	182	-0.32	0.04	0.09
	7	159	564	191	-0.19	0.14	0.03
3	0	56	-107	55	0.19	0.09	-0.03
	1	-542	1,150	-564	-1.58	-0.52	0.22
	2	104	-110	155	0.29	0.19	-0.05
	3	-494	1147	-463	-1.48	-0.42	0.21
	4	-157	275	-228	-0.58	-0.22	0.15
	5	-756	1535	-848	-2.34	-0.82	0.40
	6	-109	272	-128	-0.47	-0.13	0.13
	7	-706	1526	746	-2.23	-0.73	0.39

For error source explanation see Table 5.2.

Table 5.4. Changes of the exterior orientation elements computed by the simultaneous method

Station No	Error SOURCE	1/1000 Feet			Minutes		
		ΔX_L	ΔY_L	ΔZ_L	$\Delta\omega$	$\Delta\phi$	$\Delta\kappa$
1	0	0	12	3	-0.32	0.08	-0.05
	1	-415	139	-165	3.02	-6.13	1.69
	2	41	-20	261	0.65	5.15	-1.37
	3	-373	107	92	3.93	-1.05	0.37
	4	277	-85	47	2.64	6.34	-1.86
	5	-137	41	-122	5.97	0.13	-0.13
	6	319	-118	305	3.61	11.41	-3.18
	7	-95	9	136	6.94	5.21	-1.45
2	0	-1	-1	0	0.09	-0.01	-0.04
	1	110	196	314	1.23	4.46	-5.36
	2	50	12	224	-0.43	-2.01	3.14
	3	161	210	539	0.72	2.46	-2.18
	4	42	-162	-195	5.00	2.98	0.29
	5	153	35	119	6.14	7.45	-5.03
	6	93	-148	28	4.48	0.97	3.47
	7	204	49	343	5.63	5.44	-1.85
3	0	-1	6	-2	-0.42	-0.01	0.13
	1	-219	230	-92	0.55	1.20	-0.31
	2	3	-17	72	7.39	1.25	1.45
	3	-214	207	-18	8.36	2.46	1.00
	4	74	-46	-20	3.15	4.17	-1.03
	5	-144	177	-111	4.12	5.38	-1.47
	6	79	-70	53	10.96	5.43	0.28
	7	-139	154	-37	11.93	6.64	-0.16

For error source explanation see Table 5.2.

terior orientation elements (Table 5.4). However, in the sequential method the change in the frontal nodal point coordinates, due to this error, is substantially more significant than in the orientation angles. The simultaneous method appears to have a tendency to give better results than the sequential method under all assumed error conditions. It is remarkable that both methods provide about the same accuracy under random error conditions. Both methods also give about the same results under combined random and lens distortion error conditions.

A conclusion from the above analysis is that for the chosen geometric configuration a precise camera well calibrated gives about the same results via the sequential or simultaneous adjustment. Using a camera which has problems with the autocollimation point, the simultaneous method gives substantially better results. In any case, where no errors appear on the observations, the simultaneous method has been established as being superior. When small gross errors exist in the observations (are to say low resolution, adverse weather conditions, wrong targeting, etc.) the sequential method is less influenced by the presence of such a gross error.

6.0 PRACTICAL EVALUATION

6.1 The Gabion Wall Monitoring Project

The test area is a Gabion Wall which has been built as a part of Interstate Highway 90 East, at Snoqualmie Pass in the State of Washington (Flint, 1975: Sun, 1976; Veress and Sun, 1978; Veress, Jackson and Hatzopoulos, 1979). A KA-2, 24 inch focal length camera was modified so as to be used for terrestrial exposures, as well as to accept glass plates, has been reported by Flint, 1975. Flint, also established the terrestrial camera platforms and part of the control field.

For the present research, aerial photography has been introduced. There are four sets of aerial photography available, the dates of the exposure being: October 27, 1976; April 12, 1977; September 19, 1978 and May 14, 1979.

The aerial camera used for the photography of October 27, 1976 and April 12, 1977, is a Wild RC5/RC8 with 6 inches focal length and average resolution of 52 pair lines per millimetre. The aerial camera used for the photography of September 19, 1978 and May 14, 1979, was an Aero/View 600 with a Fairchild Ericon lens of 6 inches focal length and average resolution of 61 pair lines per millimetre. The Wild RC5/RC8 camera, was mounted in its regular position in the aeroplane floor, which is generally used for typical vertical aerial photography. In order to take the oblique photographs of the Gabion Wall structure, the aeroplane was rotated around its flight line axis. The Aero/View camera was mounted on a rotating platform on the floor of the aeroplane, and the view of the structure was provided through the aeroplane door opening, the door being removed before leaving the airport. The three first sets of aerial photography provide an image scale slightly smaller than desirable and, therefore, some of the targets are not clearly identifyable. In the last set of aerial photography, there is a desirable image scale and the photographs are of optimum quality. From a total of 38 measured targets in the October 27, 1976 set, 17 (or 45%) are imaged in the aerial photograph. In the April 12, 1977 set, there are 33 targets with 13 images (or 39%) in the aerial photograph. In the September 19, 1978 set, there are 40 measured targets with 10 images (or 25%) in the aerial photograph. Finally in the May 14, 1979 set, there are 36 measured targets with 27 images (or 75%) in the aerial photograph.

6.2 Methodology

The problems which exist in the Gabion Wall monitoring project require a proper methodology so as to obtain a satisfactory solution. The standard bundle method, however, is capable of eliminating most of these problems. Using appropriate weights for the observations, the effect of a small observation error is minimized. The problem arising from the control point observation error is very difficult to solve by any method and, therefore, it should be expected that some small absolute orientation errors will remain between the sets. This typically has a greater effect in the structural deformation measurements which require all subsequent exposures to have precisely the same absolute orientation in order to be compatible. The absolute orientation between the sets is also affected by the inherent systematic error which has to be, for the monitoring case, the same in each set of survey. This of course does not exist in the present evaluation since the equipment used was modified or substituted with other and the aerial photography was not of a constant quality during the three year period of the survey.

The present methodology applied to detect and eliminate observation blunders is as follows: a) The output from the sequential method run including error is analyzed in terms of the residuals from the intersection of a point. These residuals define whether the mathematically reconstructed corresponding light rays converge to a point. An observation, with a relatively large error, will create large residuals for the intersection and, therefore, a large a posteriori variance factor. From the intersection of a point, however, the variance factor is examined. If only two images are involved in the intersection, they are disregarded whereas, if three or more images are involved in the intersection, the one with the highest residual error is examined after appropriate statistical tests. In this way, large blunders can easily be detected and removed prior to the simultaneous adjustment. b) The simultaneous adjustment method is performed by fixing seven parameters only. One or more computations take place so that finally to obtain a posteriori variance not significantly different from the a priori value. The residuals U_i then are examined and if they are greater to the a priori assumed weight σ_{ui}, a hypothesis test $H_{\alpha i}$ is performed (Baarda, 1968; Utolia, 1975). The $H_{\alpha i}$ hypothesis is that there is a blunder in the i^{th} observation.

If

$$\left|\frac{U_i}{\sigma_{ui}}\right| > F^{1/2}_{1}, \infty, 1-\alpha_0$$

then do not reject $H_{\alpha i}$. In the present case the significance level α_0 assumed as 0.05 or 5% the F-distribution function is taken from tables (Baarda, 1968) as a function of the α_0, β_0 the β_0 is assumed here as 0.80.

In this way the blunders are eliminated and there is a final computation made where more observations can be given less reliability. In the present research, the seven fixed parameters were: the three coordinates of each of the control points 992, 993 and the Z-coordinate of the control point 884 (see previous final technical report). In the final computation the X and Y coordinates of the control point 884 were constrained within the tolerance of their standard errors determined by geodetic observations.

It should be noticed that when constraining more than seven parameters the a posteriori unit variance is tested as compared to the unit variance obtained by fixing seven parameters. To accept the constrained adjustment, there should not be any significant difference between the two variances.

6.3 Evaluation of the Monitoring Results

The final outputs from the simultaneous adjustment program are listed in the Tables 6.1 through 6.5. Each of these tables have 13 columns. The 1^{st} column indicates the sequence number of the point. The 2^{nd} column indicates the name of the point. The 3^{rd} through 8^{th} columns indicate the coordinates and the standard errors of the points with the sequence: X, σ_X, Y, σ_Y, Z, σ_Z. The columns 9, 10 and 11, represent the differences between the a priori observed or estimated ground coordinates and the final computed values. The 12th column indicates the photographs where the point was imaged and observed, for example, in the October 27, 1976 set, the point 883 was imaged and observed in the photographs No. 1, 2, 3, 4, and 5. The numbers 1, 2, 3, 4 represent the four terrestrial stations and the number 5 represents the aerial platform. Finally, column 13 indicates the date of the survey.

To determine the precision of the system, the averages of the standard errors were computed and found to be as follows:

October 27, 1976, 45% of points have aerial images

$S_X = \pm 5mm$

$S_Y = \pm 4mm$

$S_Z = \pm 12mm$

April 12, 1977, 39% of points have aerial images

$S_X = \pm 4mm$

$S_Y = \pm 3mm$

$S_Z = \pm 6mm$

September 19, 1978, 25% of points have aerial images

$S_X = \pm 6mm$

$S_Y = \pm 5mm$

$S_Z = \pm 21mm$

May 14, 1979, 75% of points have aerial images

$S_X = \pm 6mm$

$S_Y = \pm 6mm$

$S_Z = \pm 10mm$

The inclusion of the aerial photograph leads to significant improvements as is expected from the simulation experiment. The set of

Table 6.1. October 27, 1976 final output of program PHOMO

THE CORRECTED GROUND COORDINATES AND THEIR STANDAR ERROR IN METRES ARE

SN	PN	X	SX	Y	SY	Z	SZ	DX	DY	DZ	CSN	DATE
1	992	1429.626	.000	1029.340	.000	-1647.646	.000	-.000	-.000	.000	432	OCT 27
2	993	1495.512	.000	1026.655	.000	-1660.281	.000	.000	.000	-.000	4321	OCT 27
3	864	1432.492	.005	1096.625	.002	-1762.655	.000	.001	-.000	-.000	4321	OCT 27
4	882	1415.071	.005	1082.933	.003	-1738.664	.010	-.037	.294	-.182	54321	OCT 27
5	883	1435.390	.005	1069.493	.003	-1751.246	.009	.005	.315	-.039	54321	OCT 27
6	010	1428.502	.005	1003.038	.004	-1598.492	.011	-.000	-.022	-.000	542	OCT 27
7	016	1443.144	.005	1003.852	.003	-1601.889	.010	.003	-.017	.006	5421	OCT 27
8	018	1445.249	.005	999.493	.004	-1601.705	.010	-.005	-.002	-.000	5421	OCT 27
9	041	1458.094	.004	1004.520	.003	-1605.180	.009	.005	-.020	.010	5421	OCT 27
10	042	1458.060	.004	1002.659	.003	-1604.761	.009	.002	-.013	.004	5421	OCT 27
11	067	1502.462	.004	1007.118	.003	-1615.019	.008	.015	-.036	.019	541	OCT 27
12	991	1336.685	.007	1067.020	.006	-1691.922	.019	-.039	.161	.129	21	OCT 27
13	881	1328.267	.008	1076.318	.006	-1700.056	.018	-.028	-.014	-.065	521	OCT 27
14	043	1456.080	.004	1000.793	.003	-1604.483	.010	-.007	.001	.012	521	OCT 27
15	044	1458.032	.004	999.006	.003	-1604.233	.010	-.009	.010	.014	521	OCT 27
16	084	1517.406	.004	1005.666	.003	-1617.989	.010	.004	-.029	.025	543	OCT 27
17	008	1413.620	.006	1002.201	.004	-1595.280	.013	.034	.013	.078	542	OCT 27
18	009	1413.383	.006	998.653	.004	-1594.777	.013	.038	.033	.088	542	OCT 27
19	011	1428.541	.005	1001.120	.004	-1598.263	.011	.025	.014	.064	542	OCT 27
20	012	1428.464	.005	999.287	.004	-1597.972	.011	.027	.025	.070	542	OCT 27
21	060	1487.484	.004	1006.074	.003	-1611.738	.008	-.004	-.028	.009	542	OCT 27
22	102	1532.657	.004	1008.528	.003	-1621.831	.009	-.005	-.041	.014	431	OCT 27
23	203	1569.151	.005	1007.504	.004	-1629.569	.013	-.003	-.037	.032	43	OCT 27
24	523	1606.870	.007	1010.255	.005	-1638.018	.017	.002	-.055	.027	431	OCT 27
25	101	1547.364	.005	1009.136	.004	-1625.057	.010	-.001	-.048	.019	41	OCT 27
26	201	1562.323	.006	1009.912	.004	-1626.439	.013	-.010	-.049	.033	31	OCT 27
27	005	1370.245	.008	1000.026	.006	-1585.479	.019	.065	.013	-.196	21	OCT 27
28	013	1428.666	.005	997.266	.004	-1597.740	.011	.012	.039	.004	42	OCT 27
29	086	1517.538	.004	1003.933	.003	-1617.815	.009	-.012	-.018	-.022	43	OCT 27
30	088	1517.617	.004	1002.154	.003	-1617.597	.009	-.012	-.009	-.025	43	OCT 27
31	097	1525.321	.004	1003.357	.003	-1619.388	.009	-.012	-.017	-.019	43	OCT 27
32	225	1598.947	.007	1008.881	.005	-1636.118	.016	.001	-.061	.038	43	OCT 27
33	302	1576.956	.006	1010.530	.004	-1631.714	.014	-.001	-.065	.026	43	OCT 27
34	303	1576.971	.006	1008.758	.004	-1631.434	.014	-.002	-.056	.022	43	OCT 27
35	304	1583.962	.006	1008.223	.005	-1632.906	.015	-.001	-.054	.025	43	OCT 27
36	305	1577.053	.006	1007.181	.005	-1631.146	.014	-.003	-.048	.017	43	OCT 27
37	402	1591.330	.006	1011.080	.005	-1634.640	.015	.001	-.071	.036	43	OCT 27
38	113	1554.520	.005	1006.805	.004	-1626.252	.012	-.007	-.042	.002	43	OCT 27

THE MEAN SQUARE VALUE OF THE X-CORRECTIONS IS .0186
THE MEAN SQUARE VALUE OF THE Y-CORRECTIONS IS .0820
THE MEAN SQUARE VALUE OF THE Z-CORRECTIONS IS .0577

Table 6.2. April 12, 1977 final output of program PHOMO

THE CORRECTED GROUND COORDINATES AND THEIR STANDAR ERROR IN METRES ARE

SN	PN	X	SX	Y	SY	Z	SZ	DX	DY	DZ	CSN	DATE
1	992	1429.626	.000	1029.340	.000	-1647.646	.000	-.000	.000	-.000	5431	APR 12
2	993	1495.512	.000	1026.655	.000	-1660.281	.000	.000	-.000	.000	54321	APR 12
3	884	1432.481	.004	1096.625	.002	-1762.655	.000	-.010	-.000	.000	5321	APR 12
4	882	1415.059	.005	1082.893	.003	-1738.675	.007	-.049	.284	-.193	51	APR 12
5	883	1435.377	.004	1069.483	.003	-1751.244	.006	-.008	.305	-.007	5421	APR 12
6	010	1428.498	.004	1003.033	.003	-1598.476	.004	.011	-.007	-.017	541	APR 12
7	016	1443.146	.004	1003.859	.002	-1601.893	.005	.010	-.013	-.013	5421	APR 12
8	018	1445.248	.003	999.501	.003	-1601.721	.004	.012	.004	-.015	5421	APR 12
9	041	1456.095	.003	1004.524	.002	-1605.176	.004	.017	-.018	-.006	421	APR 12
10	043	1458.079	.003	1000.799	.003	-1604.503	.005	.006	-.003	-.024	542	APR 12
11	067	1502.455	.003	1007.100	.002	-1615.008	.005	.012	-.036	.017	421	APR 12
12	866	1546.587	.004	1033.835	.003	-1664.456	.008	.016	-.020	.007	31	APR 12
13	101	1547.361	.003	1009.153	.003	-1625.137	.005	.007	-.046	.006	541	APR 12
14	523	1606.907	.007	1010.239	.004	-1638.238	.012	.003	-.067	.008	31	APR 12
15	102	1532.844	.003	1008.528	.003	-1621.855	.005	-.006	-.040	.009	431	APR 12
16	203	1569.147	.004	1007.489	.003	-1629.687	.006	-.018	-.041	.009	41	APR 12
17	044	1458.045	.004	999.010	.003	-1604.260	.005	-.000	.033	.004	51	APR 12
18	065	1370.215	.007	1000.061	.004	-1585.407	.010	.030	.058	-.106	21	APR 12
19	068	1413.618	.005	1002.209	.003	-1595.302	.007	-.003	.036	-.057	42	APR 12
20	060	1487.498	.003	1006.075	.002	-1611.696	.005	-.014	-.015	-.053	42	APR 12
21	061	1487.692	.003	1004.172	.003	-1611.271	.005	-.018	-.010	-.062	42	APR 12
22	066	1399.353	.005	1001.545	.003	-1592.082	.007	.052	.049	.055	54	APR 12
23	062	1487.770	.003	1002.370	.003	-1611.030	.005	-.002	.002	.017	42	APR 12
24	201	1562.341	.005	1009.903	.003	-1628.559	.009	-.028	-.053	.056	31	APR 12
25	064	1517.409	.003	1005.656	.003	-1617.998	.006	-.012	-.022	-.037	43	APR 12
26	066	1517.544	.003	1003.929	.002	-1617.833	.006	-.013	-.013	-.039	43	APR 12
27	068	1517.609	.003	1002.159	.002	-1617.593	.006	-.014	-.004	-.044	43	APR 12
28	097	1525.316	.003	1003.359	.003	-1619.431	.006	-.014	-.011	-.038	43	APR 12
29	302	1576.962	.004	1010.519	.003	-1631.783	.007	-.011	-.053	.002	43	APR 12
30	303	1576.968	.004	1008.746	.003	-1631.517	.007	-.013	-.044	-.004	43	APR 12
31	402	1591.346	.004	1011.066	.004	-1634.917	.008	-.012	-.057	.013	43	APR 12
32	304	1583.967	.004	1008.205	.003	-1633.035	.006	-.008	-.038	-.009	543	APR 12
33	042	1458.051	.003	1002.652	.002	-1604.751	.004	-.006	.012	-.024	41	APR 12

THE MEAN SQUARE VALUE OF THE X-CORRECTIONS IS .0176
THE MEAN SQUARE VALUE OF THE Y-CORRECTIONS IS .0793
THE MEAN SQUARE VALUE OF THE Z-CORRECTIONS IS .0474

Table 6.3. September 19, 1978 output of program PHOMO.

THE CORRECTED GROUND COORDINATES AND THEIR STANDAR ERROR IN METRES ARE

SN	PN	X	SX	Y	SY	Z	SZ	DX	DY	DZ	CSN	DATE
1	992	1429.626	.000	1029.340	.000	-1647.646	.000	-.000	.000	-.000	5432	SEP 19
2	993	1495.512	.000	1026.655	.000	-1660.281	.000	.000	-.000	.000	532	SEP 19
3	884	1432.490	.005	1096.625	.002	-1762.655	.000	-.001	-.000	.000	4321	SEP 19
4	041	1458.095	.004	1004.482	.003	-1605.124	.009	.030	.000	-.003	421	SEP 19
5	101	1547.354	.007	1009.124	.005	-1625.054	.025	.069	-.003	.092	541	SEP 19
6	523	1606.914	.015	1010.247	.007	-1638.100	.040	-.069	-.039	.040	31	SEP 19
7	886	1546.574	.006	1033.812	.005	-1664.443	.024	.003	-.043	.020	41	SEP 19
8	044	1458.033	.004	998.982	.003	-1604.207	.011	.009	.032	-.033	21	SEP 19
9	991	1336.760	.005	1067.039	.005	-1692.012	.022	.036	.180	.037	21	SEP 19
10	161	1307.755	.006	1008.605	.007	-1594.501	.027	.041	.063	-.538	21	SEP 19
11	162	1308.250	.006	1006.398	.007	-1594.341	.026	.040	.075	-.556	21	SEP 19
12	163	1307.813	.006	1004.463	.007	-1593.884	.026	.039	.085	-.572	21	SEP 19
13	164	1308.253	.006	1003.230	.007	-1593.665	.026	.039	.091	-.579	21	SEP 19
14	173	1339.604	.005	1004.899	.006	-1603.372	.021	.036	.089	-.442	21	SEP 19
15	174	1339.669	.005	1002.865	.006	-1603.065	.021	.037	.100	-.460	21	SEP 19
16	018	1445.248	.003	999.479	.003	-1601.604	.007	-.002	.034	-.026	421	SEP 19
17	181	1364.083	.004	1011.455	.005	-1610.479	.016	-.025	.045	-.122	421	SEP 19
18	182	1363.354	.004	1009.308	.005	-1609.924	.016	-.026	.058	-.133	421	SEP 19
19	183	1363.188	.004	1007.027	.005	-1609.590	.017	-.032	.062	-.137	21	SEP 19
20	201	1562.326	.009	1009.893	.006	-1628.435	.028	.015	-.026	.107	531	SEP 19
21	006	1399.367	.004	1001.488	.005	-1592.034	.010	.022	.030	.027	542	SEP 19
22	042	1458.059	.003	1002.618	.003	-1604.709	.008	-.006	.010	-.075	42	SEP 19
23	043	1458.054	.003	1000.783	.003	-1604.261	.008	-.003	.020	-.009	42	SEP 19
24	060	1467.488	.004	1006.038	.003	-1611.617	.013	-.007	-.014	-.078	542	SEP 19
25	067	1502.444	.004	1007.072	.004	-1614.961	.016	-.008	-.021	-.122	42	SEP 19
26	084	1517.295	.005	1007.615	.004	-1618.214	.019	-.002	-.019	-.063	43	SEP 19
27	066	1517.404	.005	1005.650	.004	-1617.930	.019	-.004	-.007	-.073	43	SEP 19
28	097	1525.324	.005	1003.341	.004	-1619.364	.020	-.004	.006	-.036	43	SEP 19
29	102	1532.862	.006	1008.507	.004	-1621.770	.022	.009	-.023	-.079	543	SEP 19
30	302	1576.976	.009	1010.503	.006	-1631.737	.031	.018	-.033	-.115	543	SEP 19
31	303	1576.980	.009	1008.728	.006	-1631.453	.030	.016	-.021	-.111	543	SEP 19
32	304	1583.979	.010	1008.194	.006	-1632.946	.032	.017	-.020	-.117	543	SEP 19
33	089	1517.609	.005	1002.144	.005	-1617.535	.019	-.005	.013	-.084	43	SEP 19
34	402	1591.363	.010	1011.042	.006	-1634.895	.033	.022	-.036	-.071	43	SEP 19
35	225	1596.991	.011	1008.354	.007	-1636.181	.035	.023	-.024	-.080	43	SEP 19
36	171	1339.048	.005	1010.243	.006	-1604.087	.021	-.033	.061	-.139	21	SEP 19
37	172	1339.200	.005	1007.279	.006	-1603.598	.021	.058	.056	-.456	21	SEP 19
38	008	1413.651	.004	1002.184	.005	-1595.188	.008	.008	.025	-.003	42	SEP 19
39	010	1428.439	.003	1002.546	.003	-1598.332	.007	-.001	.019	-.022	42	SEP 19
40	184	1363.164	.004	1005.279	.006	-1609.329	.017	.042	.090	.051	42	SEP 19

THE MEAN SQUARE VALUE OF THE X-CORRECTIONS IS .0285
THE MEAN SQUARE VALUE OF THE Y-CORRECTIONS IS .0533
THE MEAN SQUARE VALUE OF THE Z-CORRECTIONS IS .2287

Table 6.4. May 14, 1979 final output of program PHOMO.

THE CORRECTED GROUND COORDINATES AND THEIR STANDAR ERROR IN METRES ARE

SN	PN	X	SX	Y	SY	Z	SZ	DX	DY	DZ	CSN	DATE
1	992	1429.626	.000	1029.340	.000	-1647.646	.000	-.000	-.000	.000	532	MAY 14
2	993	1495.512	.000	1026.655	.000	-1660.281	.000	.000	.000	-.000	543	MAY 14
3	664	1432.496	.005	1096.625	.002	-1762.655	.000	.005	-.000	.000	432	MAY 14
4	016	1443.156	.003	1003.829	.003	-1601.837	.006	-.037	-.054	-.051	543	MAY 14
5	041	1458.104	.004	1004.502	.004	-1605.105	.007	-.031	-.044	-.038	52	MAY 14
6	042	1458.048	.003	1002.624	.006	-1604.753	.008	.034	-.072	.050	42	MAY 14
7	043	1458.068	.003	1000.761	.004	-1604.487	.008	-.035	-.048	-.072	42	MAY 14
8	866	1546.607	.003	1033.815	.005	-1664.333	.011	.036	-.040	.130	54	MAY 14
9	006	1399.375	.005	1001.487	.005	-1592.042	.007	.015	.008	.029	542	MAY 14
10	060	1487.496	.004	1006.040	.004	-1611.652	.009	-.009	-.003	.030	54	MAY 14
11	067	1502.452	.005	1007.066	.004	-1614.933	.013	-.011	-.010	.051	42	MAY 14
12	161	1307.647	.011	1006.621	.009	-1594.328	.011	.190	.121	.183	52	MAY 14
13	162	1308.332	.011	1006.369	.009	-1594.202	.012	.180	.137	.166	52	MAY 14
14	163	1307.900	.011	1004.488	.009	-1593.753	.012	.191	.147	.170	52	MAY 14
15	164	1308.335	.011	1003.247	.009	-1593.528	.012	.165	.155	.169	52	MAY 14
16	171	1339.091	.009	1010.246	.009	-1604.025	.013	.104	.093	.124	52	MAY 14
17	173	1339.656	.009	1004.694	.007	-1603.240	.010	.229	-.754	.221	52	MAY 14
18	066	1517.397	.003	1005.644	.004	-1617.954	.008	-.017	-.023	.000	543	MAY 14
19	068	1517.522	.003	1003.925	.004	-1617.802	.008	-.018	-.016	.003	543	MAY 14
20	069	1517.607	.003	1002.146	.004	-1617.590	.008	-.014	-.005	.019	54	MAY 14
21	097	1525.312	.003	1003.334	.004	-1619.403	.008	-.022	-.016	.014	43	MAY 14
22	102	1532.829	.004	1008.508	.005	-1621.603	.009	-.022	-.037	-.026	54	MAY 14
23	101	1547.364	.003	1009.136	.005	-1625.068	.008	-.021	-.050	-.044	54	MAY 14
24	203	1569.151	.004	1007.488	.006	-1629.580	.010	-.011	-.029	-.008	54	MAY 14
25	302	1576.987	.004	1010.509	.006	-1631.634	.011	.013	-.045	.029	43	MAY 14
26	018	1445.240	.003	999.484	.004	-1601.701	.007	.004	.027	.047	542	MAY 14
27	181	1364.115	.006	1011.473	.006	-1610.391	.009	.016	.014	.020	542	MAY 14
28	183	1363.230	.007	1007.039	.006	-1609.515	.009	.019	.026	.028	52	MAY 14
29	009	1413.653	.004	1002.195	.004	-1595.215	.007	.001	.009	.015	432	MAY 14
30	304	1584.003	.004	1006.203	.006	-1632.850	.011	-.020	-.045	-.066	43	MAY 14
31	523	1606.936	.005	1010.235	.007	-1637.940	.013	-.014	-.060	-.065	43	MAY 14
32	172	1339.263	.008	1007.239	.007	-1603.527	.010	.037	.028	-.004	52	MAY 14
33	182	1363.401	.012	1009.314	.007	-1609.847	.014	.024	.006	.018	54	MAY 14
34	184	1363.204	.009	1005.278	.006	-1609.281	.011	.062	.035	.067	54	MAY 14
35	064	1517.296	.003	1007.606	.004	-1616.273	.007	-.010	-.046	-.008	54	MAY 14
36	061	1487.667	.004	1004.148	.004	-1611.247	.008	-.007	-.029	.013	54	MAY 14

THE MEAN SQUARE VALUE OF THE X-CORRECTIONS IS .0779
THE MEAN SQUARE VALUE OF THE Y-CORRECTIONS IS .1385
THE MEAN SQUARE VALUE OF THE Z-CORRECTIONS IS .0818

TABLE 6.5 PRACTICAL EVALUATION RESULTS

THE X,Y,Z-VALUES ARE IN METRES THE DX,DY,DZ ARE IN CENTIMETRES

DATE	PN	X	DX	Y	DY	Z	DZ	CSN
OCT 27	884	1432.492	.0	1096.625	.0	-1762.655	.0	4321
APR 12	884	1432.481	1.2	1096.625	.0	-1762.655	.0	5321
SEP 19	884	1432.490	.2	1096.625	.0	-1762.655	.0	4321
MAY 14	884	1432.496	-.4	1096.625	.0	-1762.655	.0	432
APR 12	006	1399.353	.0	1001.545	.0	-1592.082	.0	54
SEP 19	006	1399.367	-1.4	1001.488	5.7	-1592.034	4.8	542
MAY 14	006	1399.375	-2.3	1001.487	5.8	-1592.042	4.0	542
OCT 27	016	1443.144	.0	1003.852	.0	-1601.889	.0	5421
APR 12	016	1443.146	-.2	1003.859	-.7	-1601.893	-.4	5421
MAY 14	016	1443.156	-1.1	1003.829	2.3	-1601.857	3.2	543
OCT 27	018	1445.249	.0	999.494	.0	-1601.705	.0	5421
APR 12	018	1445.246	.1	999.501	-.8	-1601.721	-1.6	5421
SEP 19	018	1445.248	.1	999.479	1.5	-1601.664	4.2	421
MAY 14	018	1445.240	.8	999.484	1.0	-1601.701	.4	542
OCT 27	041	1458.094	.0	1004.520	.0	-1605.180	.0	5421
APR 12	041	1458.095	-.1	1004.524	-.4	-1605.176	.4	421
SEP 19	041	1458.095	-.1	1004.482	3.8	-1605.124	5.6	421
MAY 14	041	1458.104	-1.0	1004.502	1.8	-1605.106	7.4	52
OCT 27	060	1487.484	.0	1006.074	.0	-1611.738	.0	542
APR 12	060	1487.498	-1.4	1006.075	-.1	-1611.696	4.2	42
MAY 14	060	1487.496	-1.2	1006.040	3.4	-1611.652	8.7	54
OCT 27	067	1502.463	.0	1007.118	.0	-1615.019	.0	541
APR 12	067	1502.455	.7	1007.100	1.8	-1615.008	1.2	421
SEP 19	067	1502.444	1.8	1007.072	4.6	-1614.961	5.8	42
MAY 14	067	1502.452	1.0	1007.066	5.1	-1614.933	8.6	42
OCT 27	086	1517.406	.0	1005.666	.0	-1617.989	.0	543
APR 12	086	1517.409	-.3	1005.656	1.0	-1617.998	-.9	43
SEP 19	086	1517.404	.2	1005.650	1.6	-1617.930	5.9	43
MAY 14	086	1517.397	.9	1005.644	2.2	-1617.954	3.5	543
OCT 27	088	1517.538	.0	1003.933	.0	-1617.815	.0	43
APR 12	088	1517.544	-.6	1003.929	.4	-1617.833	-1.8	43
MAY 14	088	1517.522	1.6	1003.925	.8	-1617.802	1.3	543
OCT 27	089	1517.616	.0	1002.154	.0	-1617.597	.0	43
APR 12	089	1517.609	.8	1002.159	-.6	-1617.593	.4	43
MAY 14	089	1517.607	.9	1002.146	.8	-1617.590	.7	54

September 19, 1978 which has only 25% of aerial images has substantially greater standard error in the Z-direction. The May 14, 1979 set which has the best image quality, scale and resolution aerial photography from all sets does not have the maximum accuracy because of eliminating the number 1 photograph completely from this set (it was not observable). Therefore, the terrestrial parallactic angle was not as in the other sets. The best terrestrial parallactic angle is obtained by photographs taken from the stations 1 and 4. In the May 14^{th} set of data, there is a small difference between S_X, S_Y and S_Z because there is a small difference between all parallactic angles. The best results were obtained on April 12, 1977, and in this set the precision as compared to the 850 meters assumed photographic distance is of:

1:120,000

The precision is close to that predicted by the simulation experiment. The aerial photograph also makes significant improvement in the Y-direction as compared with results of the same project reported by Veress, 1977 and Veress, 1979. The improvement in the Y-direction is about 40%. The monitoring results with the measured deformations are presented by Table 6.5. Although the inherent systematic error was not constant for each set of survey, the monitoring results are satisfactory and show clearly the motion of the structure. The DX column indicates the motion along the largest dimension of the structure. The DY column represents the settlement of the structure; when positive the point moves downwards. The DZ column represents the deflection of the point, when positive it moves outwards.

7.0 ERROR ANALYSIS AND DATA PRESENTATION

7.1 Error Analysis

The variance-covariance matrix Σ of a photogrammetrically determined point is obtained as follows:

$$\Sigma = \sigma_o^2 Q_{XX} = \begin{bmatrix} \sigma_o^2 q_{XX} & \sigma_o^2 q_{XY} & \sigma_o^2 q_{XZ} \\ \sigma_o^2 q_{XY} & \sigma_o^2 q_{YY} & \sigma_o^2 q_{YZ} \\ \sigma_o^2 q_{XZ} & \sigma_o^2 q_{YZ} & \sigma_o^2 q_{ZZ} \end{bmatrix} = \begin{bmatrix} \sigma_X^2 & \sigma_{XY} & \sigma_{XZ} \\ \sigma_{XY} & \sigma_Y^2 & \sigma_{YZ} \\ \sigma_{XZ} & \sigma_{YZ} & \sigma_Z^2 \end{bmatrix} \qquad 7.1$$

The ellipsoid of constant probability is then given by the equation: (Mikhail, 1976)

$$X^T \Sigma^{-1} X = [X \ Y \ Z] \Sigma^{-1} \begin{bmatrix} X \\ Y \\ Z \end{bmatrix} = K^2 \qquad 7.2$$

When K = 1, it is called the standard ellipsoid. The semiaxes of the ellipsoid (a, b, c) are determined by diagonalizing Σ by writing:

$$\begin{bmatrix} \sigma_u^2 & 0 & 0 \\ 0 & \sigma_v^2 & 0 \\ 0 & 0 & \sigma_w^2 \end{bmatrix} = \begin{bmatrix} a^2 & 0 & 0 \\ 0 & b^2 & 0 \\ 0 & 0 & c^2 \end{bmatrix} = \begin{bmatrix} \lambda_1 & 0 & 0 \\ 0 & \lambda_1 & 0 \\ 0 & 0 & \lambda_1 \end{bmatrix} = M^T \Sigma M$$

Where M is an orthogonal matrix whose columns are the normalized eigen-vectors of Σ; λ_1, λ_2, and λ_3 are the eigen-values of Σ; and the u, v, w is a rotated coordinate system such that the random variables in the directions of its axes are uncorrelated. The probability of a point falling inside or on the ellipsoid is defined by

$$a = K\sigma_u, \quad b = K\sigma_v, \quad c = K\sigma_w$$

The expression is:

$$P\left[\left(\frac{u^2}{\sigma_u^2}+\frac{v^2}{\sigma_v^2}+\frac{w^2}{\sigma_w^2}\right)<K^2\right] = P[\chi_3^2 < K^2] = 1-\alpha$$

For the standard ellipsoid $(1-\alpha) = 0.199$ which is obtained from χ^2 with three degrees of freedom. For a point, however, the probability of falling inside or on the standard ellipsoid is 0.199. In order to establish confidence regions, we select the α level and compute the multiplier K. For example, for $\alpha = 0.05$

$$P\{\chi_3^2 < \chi_{0.05,\ 3}\} = P\{\chi_3^2 < 7.81\} = 0.95$$

and $K = \sqrt{7.81} = 2.79$

For the ellipsoid, however, where:

$$a = 2.79\sigma_u, \quad b = 2.79\sigma_v, \quad c = 2.79\sigma_w$$

the possibility of a point falling inside is 95%. (Mikhail, 1976.)

The eigen-values are the roots of the cubic equation:

$$\lambda^3 - (\sigma_X^2+\sigma_Y^2+\sigma_Z^2)\lambda^2 +$$

$$+(\sigma_X^2\sigma_Y^2+\sigma_Y^2\sigma_Z^2+\sigma_X^2\sigma_Z^2-\sigma_{XY}^2-\sigma_{YZ}^2-\sigma_{XZ}^2)\lambda -$$

$$-\ \sigma_X^2\sigma_Y^2\sigma_Z^2-2\sigma_{XY}\sigma_{YZ}\sigma_{XZ}+\sigma_X^2\sigma_{YZ}^2+\sigma_Y^2\sigma_{XZ}^2+\sigma_Z^2\sigma_{XY}^2 = 0$$

After determining the eigen-values, the eigen-vectors are determined and normalized in order to obtain the M-matrix. The error ellipsoid can then be plotted by automatic plotting devices.

For many applications the two-dimensional equivalent, error ellipse, is enough to determine the precision of the system. The formulas for the error ellipse are the same as for the error ellipsoid, except that terms which belong to two selected dimensions are retained and the third dimension terms are neglected.

For the X-Y selected directions, the Eq. 7.2 will be modified as:

$$[X\ Y]\Sigma^{-1}\begin{bmatrix}X\\Y\end{bmatrix} = K^2$$

where

$$\Sigma = \sigma_o^2\begin{bmatrix}q_{XX} & q_{XY}\\ q_{XY} & q_{YY}\end{bmatrix}$$

The principle axes and the rotation angle of the error ellipse can be determined in the way given by Veress, 1974 or in the way given by Mikhail, 1976. Here, a simple method using the Mohr circle will be described.

From Fig. 7.1, the following quantities are determined

$$a^2 = \frac{\sigma_X^2 + \sigma_Y^2}{2} + R$$

$$b^2 = \frac{\sigma_X^2 + \sigma_Y^2}{2} - R$$

Where a is the semimajor axis of the error ellipse

b is the semiminor axis of the error ellipse

R is shown in Fig. 7.1 and computed as:

$$R = \sqrt{\left(\sigma_X^2 - \frac{\sigma_X^2+\sigma_Y^2}{2}\right)^2 + \sigma_{XY}^2} = \sqrt{\frac{1}{4}(\sigma_X^2 + \sigma_Y^2) + \sigma_{XY}^2}$$

and

$$\sin 2\theta = \frac{\sigma XY}{R}$$

$$\cos 2\theta = \frac{\sigma_X^2 - \sigma_Y^2}{2}$$

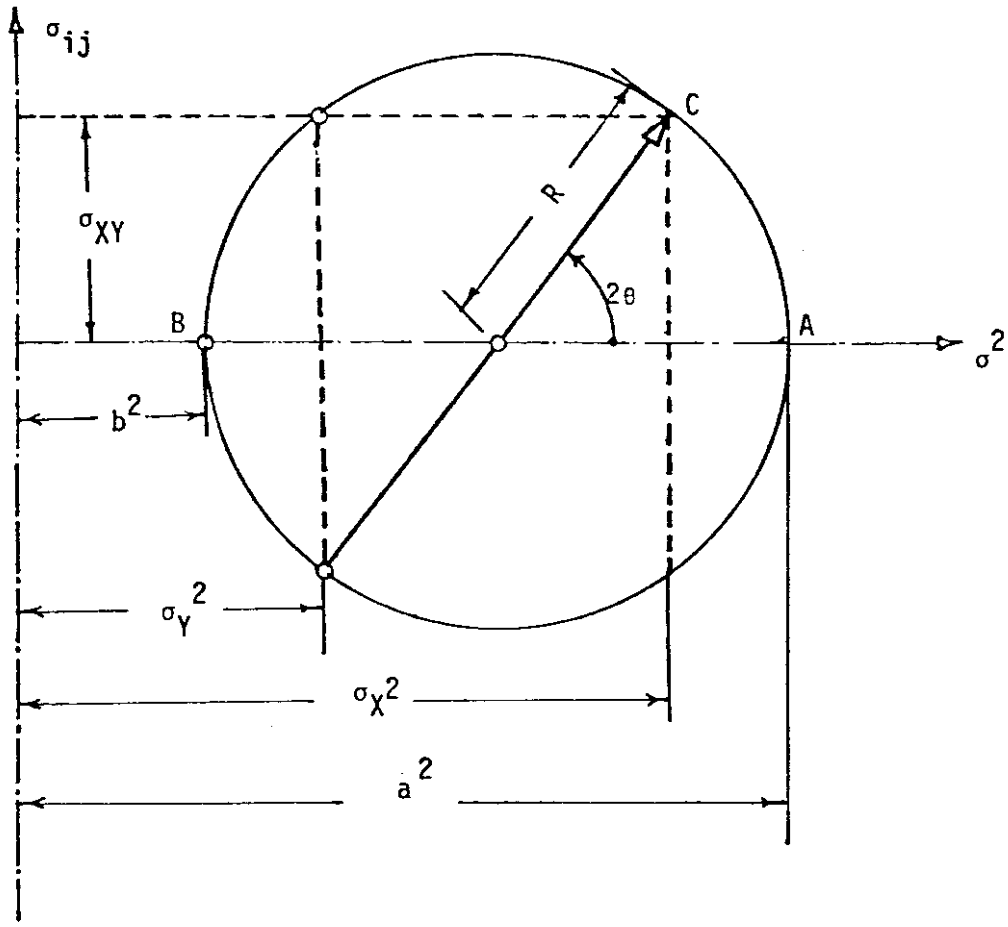

Fig. 7.1. The Mohr circle for determining the elements of the error ellipse.

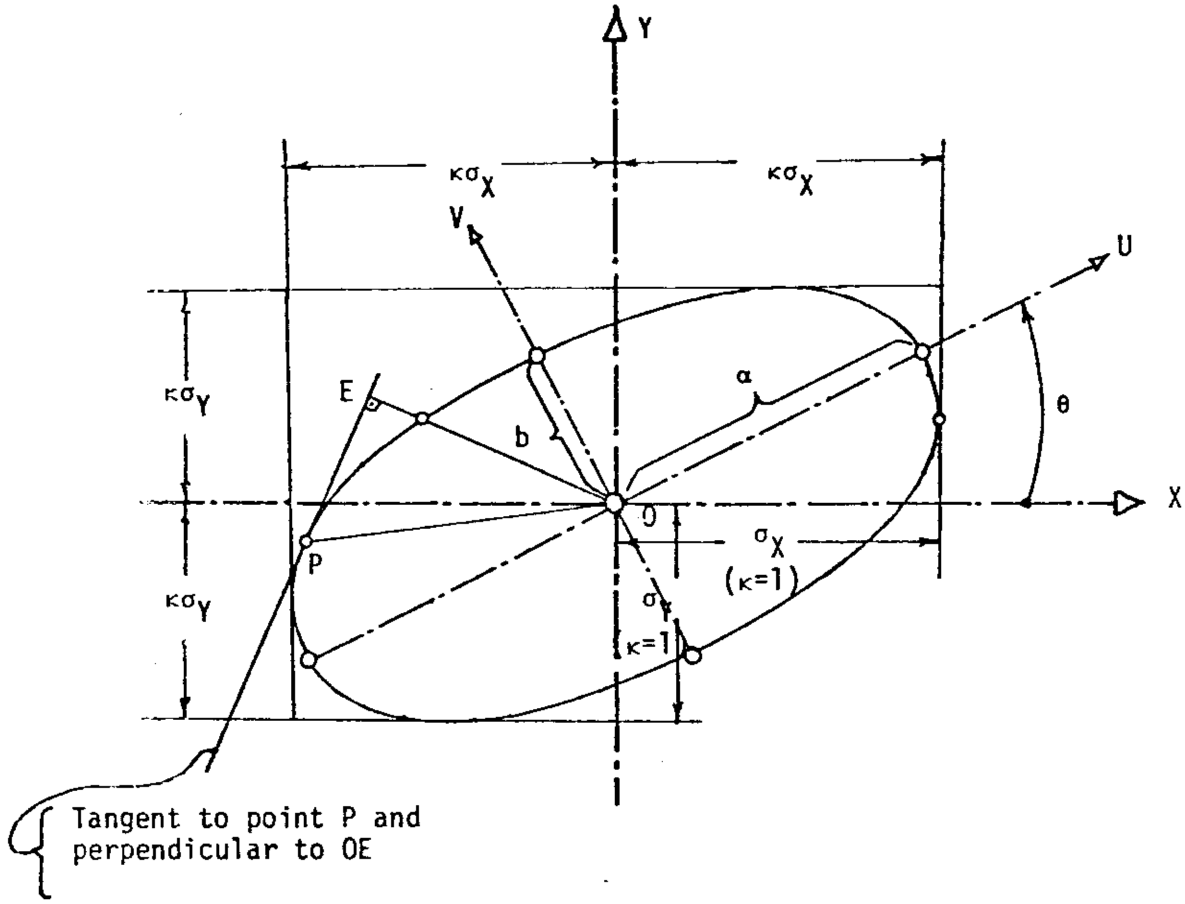

Fig. 7.2. The standard ellipse (After Mikhail, 1976)

and

$$\tan 2\theta = \frac{\sin 2\theta}{\cos 2\theta} = \frac{2\sigma_{XY}}{\sigma_X^2 - \sigma_X^2}$$

The direction of the rotation is C -A -B (Fig. 7.1).

The error ellipse is shown in Fig. 7.2. When the standard ellipse is used, it is possible to determine the standard error of any point at any direction by drawing the foot point curve (Veress, 1974). For the direction OE the standard error will be: σ_{OE} = (OE) (Fig. 7.2).

7.2 Graphical Representation of Monitoring Results.

The graphical representation of the monitoring results needs to illustrate two major kinds of output results. One is the accuracy of the system and the other is the motion of the structure. These monitoring results may be illustrated together or separately.

This presentation can be shown either by the error ellipse or by the error ellipsoid as it is analyzed in Section 7.1. The standard ellipse or any other (required from the specifications) error ellipse or foot point curve can be plotted directly from the output results.

This presentation can be applied for a selected number of points in each run so as to provide a general concept of the accuracy capabilities of the monitoring system.

Graphical representation of the structural deformation illustrates in a graph form the structural motion versus time, with three curves which represent the structural deformation in the X, Y and Z directions respectively. Erlandson and Veress, 1975a and 1976 use this type of data presentation for the case where a large number of points are monitored. This method is shown in Fig. 7.3 for the point 86.

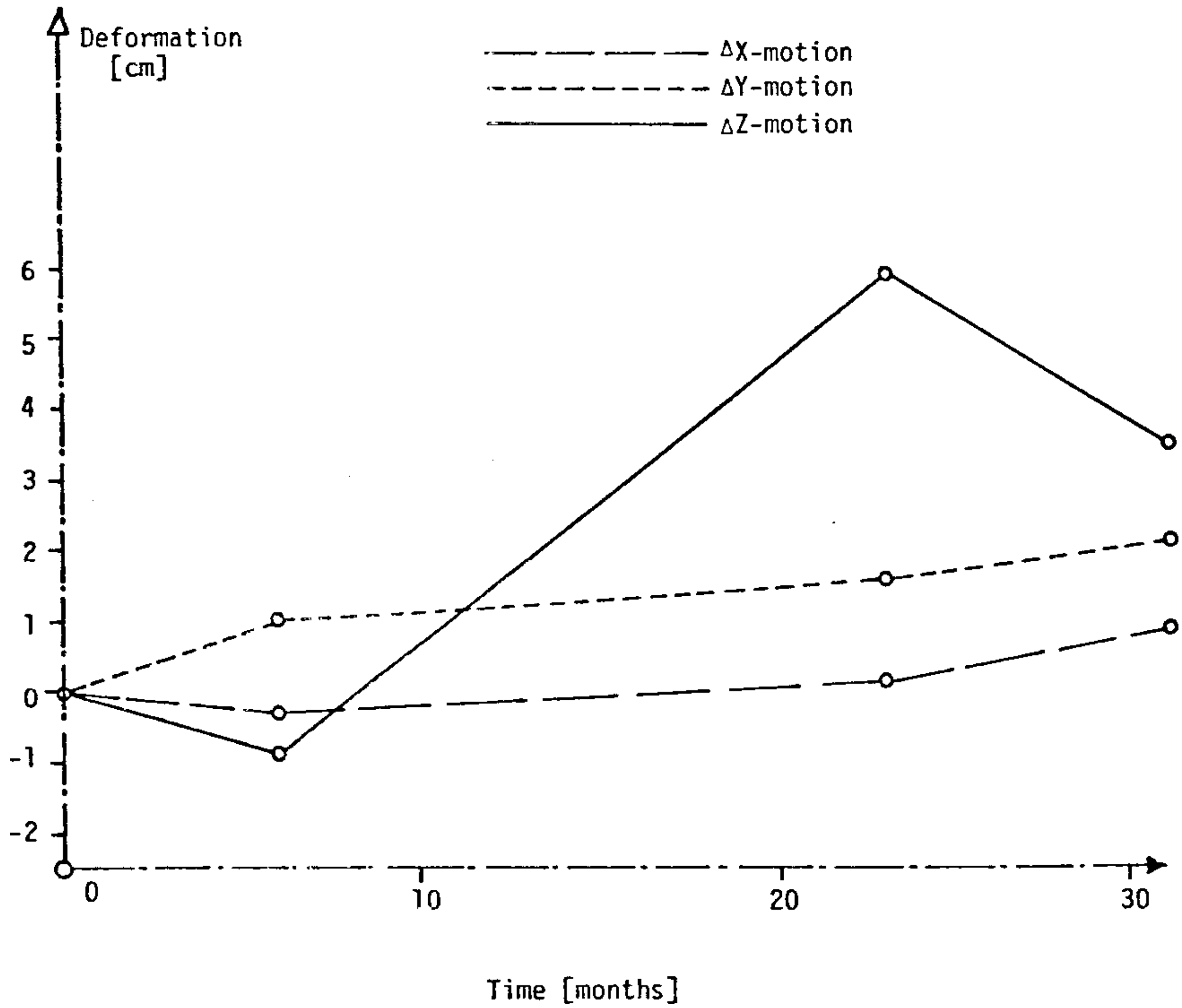

Rig. 7.3. Structural motion of the point 86.

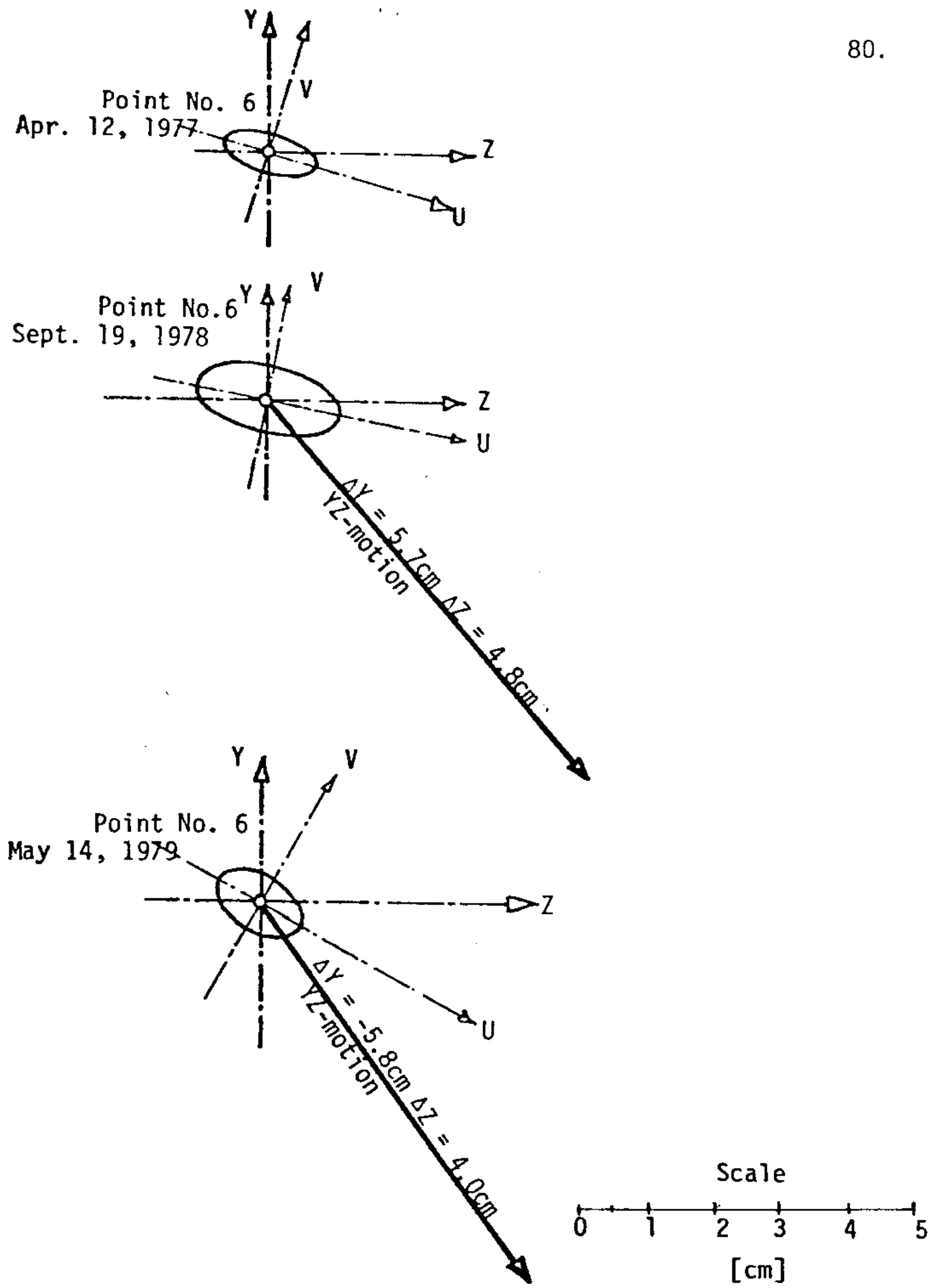

Fig. 7.4. The error ellipse and the deformation vector for point No. 6.

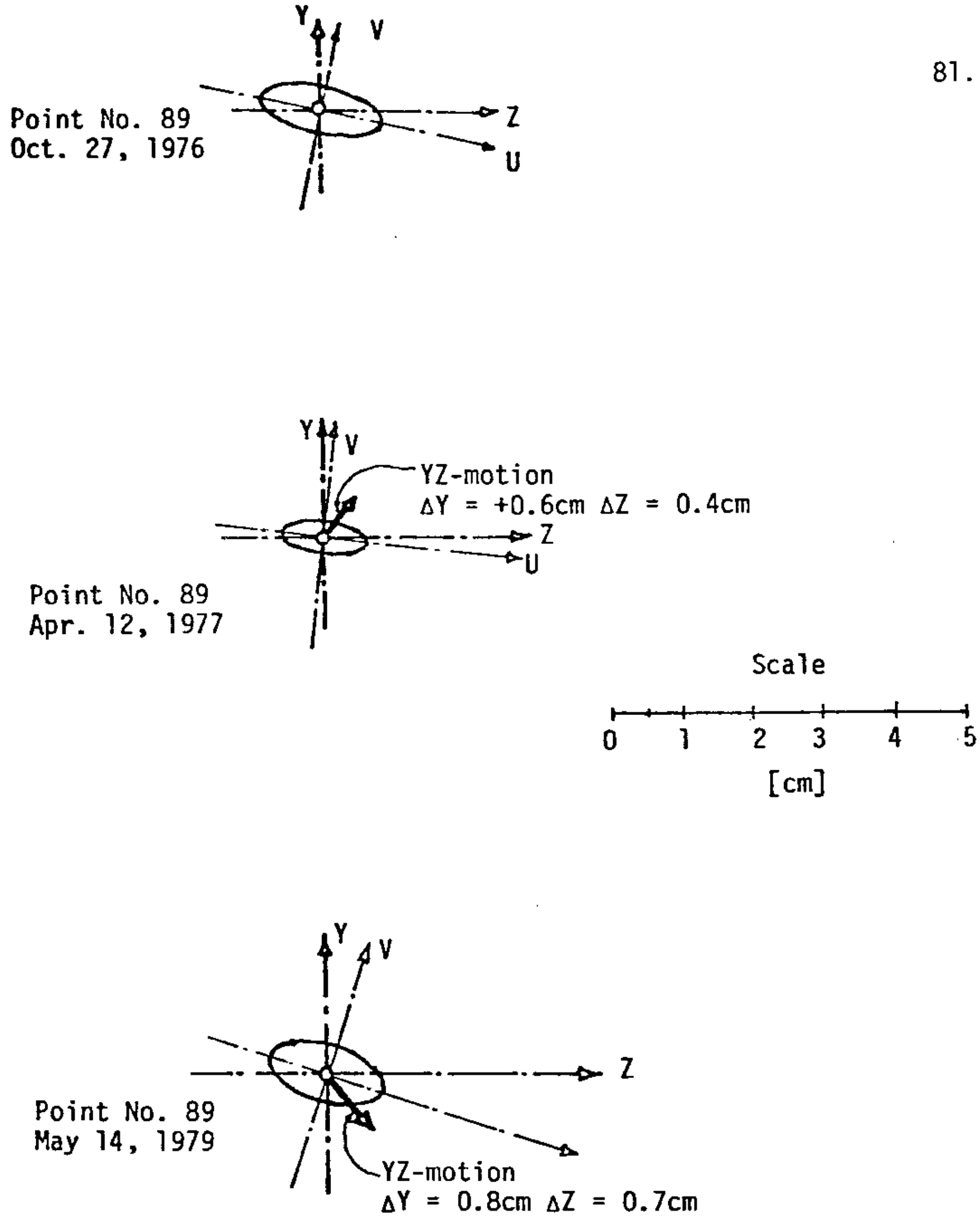

Fig. 7.5. The error ellipse and the deformation vector for point No. 89.

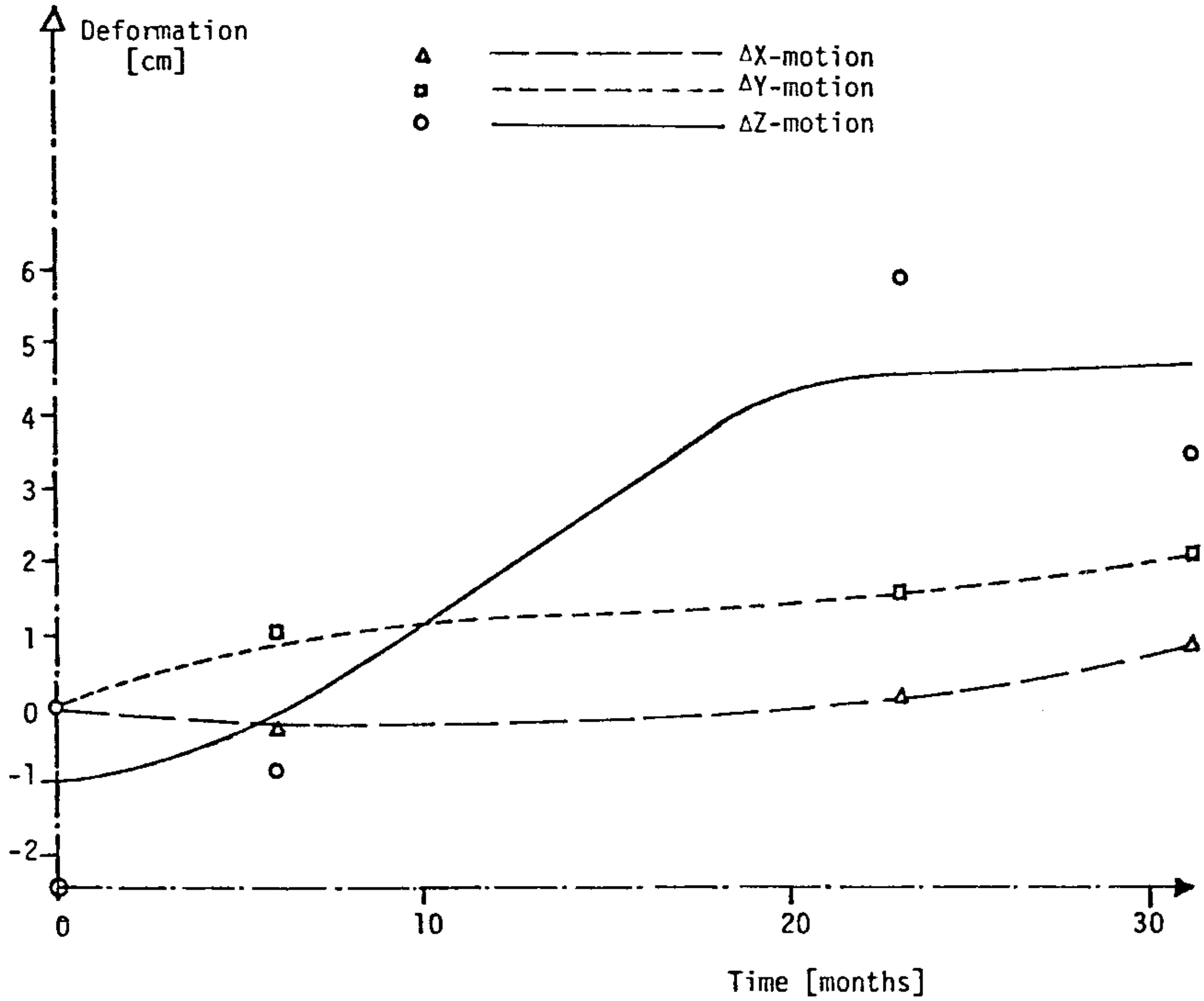

Fig. 7.6. Best fitting curve for point 86.

The combined representation of system accuracy and structural motion, can be achieved in two ways. One is as developed by Erlandson and Veress, 1976, where the error ellipse is plotted in a combination with the deformation vector. This is illustrated by Fig. 7.4 and 7.5. This technique is suggested by Erlandson and Veress, 1976, for a relatively small number of points with large deformation vectors. The interpretation of this type of presentation is that when the deformation vector falls inside the error ellipse it does not represent significant structural deformation. If the deformation vector exceeds the error ellipse limits, it represents significant structural motion. In Fig. 7.4 a deformation vector which exceeds the error ellipse limits, is shown. In Fig. 7.5 a deformation vector which is close to the error ellipse limits, is shown. The error ellipse concept can be extended to the foot point curve illustration or to the error ellipsoid. The second way of presentation is by approximating a curve which is determined so that to be the best fitting curve to the measured strucural motion. To draw this curve, knowledge and backgound of structural mechanics and soil mechanics is necessary. The deviations of the plotted points from the best fitting curve determine the accuracy of the system. In Fig. 7.6 is illustrated the best fitting curve for the point 86.

8.0 PRACTICAL APPLICATIONS OF COMPUTER PROGRAMS

8.1 SEQGE

SEQGE is a sequential computer program developed to perform the following operation:

1. Image coordinate refinement by:
   a, affine transformation
   b, conformal transformation
   c, correction to autocollimation point
   d, lens distortion correction
2. Resection by vector method.
3. Determination of orientation matrix.
4. Intersection by vector method.

The input data are:

a, average image coordinates
b, camera calibration data
c, control point coordinates
d, various parameters if they are know which may be computed by program 1, 2 and 3 of the above

The output data are:

a, X,Y,Z coordinates of measured points
b, statistical analysis (standard errors, etc.)

The SEQGE program can be used for conventional aerial trangulation, close-range photogrammetric applications, terrestrial photogrammetry using only terrestrial photographs, or a combination of aerial and terrestrial photographs.

8.2 CARVL

This program is designed for use of image coordinate refinement for measured images of photographs with a format size of 9½" x 9½". The program uses billinear transformations.

8.3 PHOMO

This is a simultaneous adjustment program. It can be used for triangulation or various combinations of aerial and terrestrial cameras. The program is capable to accommodate six photographs taken with six different kinds of cameras and fifty ground points with 200 images.

The input data is:

a, refined image coordinates

b, standard errors of observations.

c, estimated exterior orientation elements with their standard error

d, estimated ground coordinates and their standard errors

The output data is:

a, most probable values of orientation elements

b, adjusted values of ground parameters

c, the statistical data of all parameters

The program is applicable for analytical aerial triangulation, strip or block, which consists of no more than six photographs. It is specifically designed for monitoring of structures when a large number of ground points are needed with maximum accuracy photographed from a few camera stations.

9.0 CONCLUSIONS

The combination of aerial and terrestrial photogrammetry for monitoring large structures has been developed in this research. The experimental results which are analyzed in Chapter VI prove that for the present application, the aerial photography significantly increases the precision of the system, which was found to be as high as 1:120,000 of the photographic distance. The mathematical formulation, as based on the standard bundle method of adjustment, in combination with appropriate statistical tests, provides the capability of minimizing blunders from the observations and therefore an inexpensive camera such as the KA-2, for obtaining the photography can be used.

The degrees of freedom, which are increased by treating all parameters as observations with a priori variance, allow a full statistical analysis giving, therefore, valuable information about the reliability of the final results.

The introduction of the aerial photograph has greatly increased the geometric strength of the monitoring system and therefore the final results are obtained with a higher precision. There are some limits, however, which specify the optimum geometry situation in terms of parallactic angel. These limits have been established in this research, based on a simulation experiment and practical evaluation.

The method developed in this research for the monitoring of large structures is a universal method and it can include additional aerial photography. This can be a useful tool in the monitoring by photogrammetry, which has the following advantages.

1. The coordinates of a large number of points, from a remote distance, can be simultaneously determined.
2. The position of a point is fully defined in the three-dimensional space, at a certain time, with a statistically determined precision.
3. The photogrammetric monitoring system is independent from the structure, as compared to the conventional monitoring methods in use.
4. Although the terrestrial platforms have limitations in providing the optimum goemetry, depending on the terrain features, the aerial photography combined with the terrestrial can usually provide favourable geometry for the chosen situation.
5. The photogrammetric monitoring method is very economical as compared to other monitoring techniques and the economy is not significantly affected by increasing the number of the points.
6. The photographs obtained throughout the period of monitoring constitute a permanent record for the structure.

Some of the disadvantages of the photogrammetric monitoring method are:

1. The measurements are referred to points on only the surface of the structure.
2. It is a weather dependent method.

Further developments in the photogrammetric monitoring field should be increasingly oriented towards the bundle method with additional self-calibration parameters in which case the inherent systematic error does not have to be constant. Also in this way, variable pieces of equipment can be used without the necessity to establish permanent camera platforms. The weather condition problem can be overcome with special self illuminated targets and using infrared emulsion.

Finally, further research should be made to study motions of the body of the structure by photogrammetry. This can be accomplished by having two targets, the one on the surface of the structure and the other through a rod connected properly with the body of the structure. The surface target in this case records the surface motion while the body-target records surface motion, as well as body-motion and therefore by proper analysis of both targets the body motion can be determined.

REFERENCES

ABDEL-AZIZ, Y. I., ALICE, M. B.: On the Calibration of Close-Range Cameras. Presented at the ACSM/ASP Convention Washington, D. C., March 12-17, 1972.

A.S.P.: Manual of Photogrammetry. Third Edition, 1966.

ARGYRIS, J. H., AICHER, W., EBERLE, K., KIRSCHSTEIN, M.: Measuring of Three-Dimensional Deformations via Photogrammetric Methods and Electronic Data Processing. ISD-Report No. 118, Stuttgart, 1972.

BAARDA, W.: A Testing Procedure for Use in Geodetic Network. Netherlands Geodetic Commission, Publications in Geodesy, New Series, Vol. 2, No. 5, Delft, 1968 b.

BALL, W. E.: A Tensor Approach to Block Triangulation. Photogrammetric Engineering, Vol. 39, No. 1, pp. 81, January 1973.

BAUER, H. and MULLER, J.: Height Accuracy of Blocks and Bundle Adjustment with Additional Parameters. Presented Paper of Commission III, ISP Congress, Ottawa, 1972.

BJERHAMMAR, A.: Theory of Errors and Generalized Matrix Inverses. Elsevier Scientific Publishing Company. Amsterdam-London-New York, 1973.

BORCHERS, P. E.: The Photogrammetric Study of Structural Movements in Architecture. Photogrammetric Engineering, Vol. 30, No. 5, pp. 809-817, 1964.

BORISENKO, A. I., TARAPOV, I. E.: Vector and Tensor Analysis with Applications. Prentice-Hall, Inc. Englewood Cliffs, N. J., 1968.

BRANDENBERGER, A. J. and EREZ, M. T.: Photogrammetric Determination of Displacements and Deformations in Large Engineering Structures. The Canadian Surveyor, Vol. 26, No. 2, June 1972.

BROWN, D. C.: A Solution to the General Problem of Multiple Station Analytical Stereotriangulation. RCA Data Reduction, Report No. 43, 1958.

BROWN, D. C.: Decentering Distortion of Lenses. Photogrammetric Engineering, Vol. 33, No. 3, pp. 444-463, 1966.

BROWN, D. C.: Calibration of Close-Range Cameras. Presented Paper of Commission III, XII Congress of ISP, Ottawa, 1972.

BROWN, D. C.: Bundle Adjustment with Strip-and-Block-Invariant Parameters, Bul, Vol. 42, No. 6, pp. 210-220, 1974.

BROWN, D. C.: The Bundle Adjustment-Progress and Prospects. Invited Paper Commission III, XIII Congress of ISP, Helsinki, 1976.

BROWN, D. C., DAVIS, R. G. and JOHNSON, F. C.: The Practical and Rigorous Adjustment of Large Photogrammetric Nets. Technical Documentary Report RADC-TDR-64-353; RADC, New York, 1964.

DAVIS, R. G.: Analytical Adjustment of Large Blocks. Photogrammetric Engineering, March 1965.

DAVIS, R. E., FOOTE, F. S. and KELLY, J. W.: Surveying Theory and Practice. McGraw-Hill Book Co., New York, St. Louis, San Francisco, Toronto, London and Sydney, 1966.

DE GROSS, E. G.: A Study of Terrestrial Methods for Determining the Motion in Structural Highway Design. Thesis, University of Washington, 1970.

DORRER, E.: Tensor Calculus in Computational Photogrammetry. Department of Surveying Engineering, University of New Brunswick, Fredericton, N. B. Canada.

DORRER, E.: Complex Numbers for Block Adjustment. Photogrammetric Engineering, Vol. 37, No. 1, pp. 85-89, January 1971.

EREZ, M. T.: Analytical Terrestrial Photogrammetry Applied to the Measurement of Deformations in Large Engineering Structures. Dissertation, University of Laval, 1971.

ERLANDSON, J. P., PETERSON, J. C. and VERESS, S. A.: Performance of Observations of Structural Deformations by Photogrammetric Methods. Technical Report, U. S. Army Corps of Engineers, Seattle District, 1973.

ERLANDSON, J. P., PETERSON, J. C. and VERESS, S. A.: The Modification and Use of the BC-4 Camera for Measurements of Structural Deformation. Proceedings of the ASP Fall Convention, September 10-13, 1974a.

ERLANDSON, J. P. and VERESS, S. A.: Contemporary Problems in Terrestrial Photogrammetry. Photogrammetric Engineering and Remote Sensing, 1974b.

ERLANDSON, J. P. and VERESS, S. A.: Monitoring Deformations of Structures. Photogrammetric Engineering and Remote Sensing, Vol. 41, No. 11, pp. 1375-1384, November 1975.

ERLANDSON, J. P. and VERESS, S. A.: Photogrammetrische Erfassung von Bauwerksveranderungen. VR-Vermessugswesen und Raumordnung, Heft 8/1976.

ERLANDSON, J. P. and VERESS, S. A.: Methodology and Standards for Structural Surveys. Proceedings of the Symposium on Close-Range Photogrammetric Systems, July 28-August 1, 1975, pp. 575-596.

FLINT, E. E.: Design for Photogrammetric Monitoring of a Gabion Wall. Thesis, University of Washington, 1975.

FRASER, C. S.: Refraction Modelling in Terrestrial Photogrammetry. Proceedings of the A.S.P., 45th Annual Meeting, Washington D. C., Vol. 2, March 18-24, 1979a.

FRASER, C. S.: Simultaneous Multiple Camera and Multiple Focal Setting Self-Calibration in Photogrammetry. Dissertation, University of Washington, 1979b.

GALETTO, R.: A Photogrammetric Method for Assessing the Displacements Under Stress of Larger Structure Models (Theory). Bollettino de Geodesia e Scienze Affini, Vol. 27, No. 2, pp. 185-198, 1968a.

GALETTO, R., BERNINI, F. and CUNIETTI, M.: A Photogrammetric Method for Assessing the Displacements Under Stress of Large Structure Models (Experimental Applications). Bollettino de Geodesia e Scienze Affini, Vol. 27, No. 3, pp. 293-316, 1968.

GHOSH, S. K.: Phototriangulation. The Ohio State University, Lexington Books, Toronto, London, 1975.

GUTU, A.: A Photogrammetric Measurement Accuracy of Wall Pillar Cracks in Rock Salt Mines. Buletin de Fotogrammetrie, Special Issue, 1972.

HAMILTON, W. C.: Statistics in Physical Science. The Ronald Press Co., New York, 1964.

HALLERT, B.: Some Remarks Concerning the Theory of Errors for Convergent Aerial Pictures in Comparison with Near Vertical Pictures. International Archives of Photogrammetry, Vol. VII, Part 4a, Stockholm, 1956.

HALLERT, B.: Photogrammetry. McGraw-Hill Book Co., New York, Toronto and London, 1960.

HALLERT, B. and OTTOSON, L.: General Differential Formulae of the Complete Projective Relations Between Planes. International Archives of Photogrammetry, Vol. XV, Part 4, Lisbon, 1964.

HIRVONEN, R. A.: Adjustment by Least-Squares in Geodesy and Photogrammetry. Frederic Ungar Publishing Co., New York, 1965.

HOU, M. C. Y.: Aerotriangulation Precision Attainable for Highway Photogrammetry, ASP/ACSM Fall Convention, Colombus, Ohio, October 1972.

HOU, M. C. Y.: Are Three Points Necessary? Photogrammetric Engineering and Remote Sensing, 1974.

HOU, M. C. Y.: Water Dam Control Surveying and Adjustments. Proceedings of the ACSM, 39th Annual Meeting, March 18-24, Washington D.C., 1979.

KARARA, H. M. and MARKS, G. W.: Analytical Aerial Triangulation for Highway Location and Design. University of Illinois, pp. 1-227.

KELLER, M. and TEWINKEL, G. C.: Aerotriangulation Image Coordinate Refinement. Technical Bulletin, No. 25, U. S. Department of Commerce, March 1965.

KENECHNY, G.: Interior Orientation of Convergent Photography. Photogrammetric Engineering, Vol. 31, No. 4, 1965.

KENEFICK, J. F.: Ultra-Precise Analysis. Photogrammetric Engineering, Vol. 37, No. 11, pp. 1167-1187, 1971.

KENEFICK, J. F., GYER, M. S. and HARP, W. F.: Analytical Self-Calibration. Photogrammetric Engineering, Vol. 38, No. 11, pp. 1117-1126, 1972.

KUPFER, G.: Improvement of the Geometry of Aerial Photos. Photogrammetric Engineering, Vol. 38, No. 5, pp. 479-486, 1972.

MAKAROVIC, B.: Model Deformations and Their Compensational Possibilities in Affine Plotting. I. T. C. Publication A-22, Delft, 1963.

MATOS, R. A.: Multiple-Station Analytical Triangulation. Photogrammetric Engineering, Vol. 37, No. 5, pp. 173-176, 1971.

MIKHAIL, E. M.: Observations and Least-Squares. IEP Series in Civil Engineering, New York, pp. 497, 1976.

MOFFIT, F. H.: Surveying. Intext Educational Publishers, 1975.

PLANICKA, A.: Die Renutzung der Terrestrischen Photogrammetrie in Deformationsmessung von Steinschuttdammen. Paper presented at the 6th Internal Course for Engineering Surveys of High Precision, Graz, Austria, 1970.

SALMENPERA, H., ANDERSON, J. M. and SAVOLAINEN, A.: Efficiency of the Extended Mathematical Model in Bundle Adjustment. Bul., Vol. 42, No. 6, pp. 229-233, 1974.

SCHMID, H. H.: An Analytical Treatment of the Problem of Triangulation by Stereophotogrammetry. Photogrammetria, pp. 67-77 and 91-116, 1956-1957.

SCHUT, G. H.: On Correction Terms for Systematic Errors in Bundle Adjustment. Bul. Vol. 42, No. 6, pp. 223-229, 1974.

SCHUT, G. H.: Selection of Additional Parameters for Bundle Adjustment. Proceedings of the ASP Fall Meeting, Albuquerque, New Mexico, pp. 490-503, 1978.

SUN, L. L.: Photogrammetric Monitoring of a Gabion Wall. Thesis, University of Washington, 1976.

UOTILA, U. A.: Statistical Tests as Guidelines in Analysis of Adjustment of Control Nets. Surveying and Mapping, ACSM, pp. 47-52, March 1975.

VERESS, S. A.: The Effect of the Fixation Disparity of Photogrammetric Engineering, Vol. 30, No. 1, 1964.

VERESS, S. A.: Aerial Triangulation Using Independent Photo Pairs. Journal of Surveying and Mapping Division, Proceedings of the American Society of Civil Engineers, New York, 1965.

VERESS, S. A.: Model Deformation and its Effect on Attainable Accuracy. Journal of the Japan Society of Photogrammetry, Vol. 6, No. 7, 1967.

VERESS, S. A.: The Use and Adoption of Conventional Stereoplotting Instruments for Bridging and Plotting of Super Wide Angle Photography. Canadian Surveyor, Vol. 23, No. 4, Ottawa, 1969a.

VERESS, S. A.: Interim Technical Report Study of the Three-Dimensional Extension of Polluted Air, March 1969b.

VERESS, S. A.: Determination of Motion and Deflection of Retaining Walls, Part I, Theoretical Considerations. University of Washington, Final Technical Report, 1971.

VERESS, S. A. and DE GROSS, G. E.: Determination of Motion and Deflection of Retaining Walls. Part II, Technical Applications, University of Washington, Final Technical Report, 1971.

VERESS, S. A.: Adjustment by Least-Squares (Monograph). American Congress on Surveying and Mapping, Washington D. C., pp. 218, 1974.

VERESS, S. A.: Measures of Accuracy for Analysis and Design of Survey. Surveying and Mapping, Vol. 33, No. 4, pp. 435-442, December 1973.

VERESS, S. A., HOU, M. C. Y., FLINT, E. E., SUN, L. L., HATZOPOULOS, J. N., and JIJINA, C.: Photogrammetric Monitoring of a Gabion Wall. Final Technical Report, Department of Transportation, Report No. 31.1, Research Project Y-1699, September 1977.

VERESS, S. A. and SUN, L. L.: Photogrammetric Monitoring of a Gabion Wall. Photogrammetric Engineering and Remote Sensing. Vol. 44, No. 2, pp. 205-211, February 1978.

VERESS, S. A., JACKSON, N. G. and HATZOPOULOS, J. N.: Analysis of Monitoring the Gabion Wall by Inclinometer and Photogrammetry. Proceedings of the ASP, 45th Annual Meeting, Washington D. C., pp. 216-237, March 18-24, 1979.

WOLF, P. R.: Elements of Photogrammetry. McGraw-Hill, Inc., 1974.

WONG, K. W.: Mathematical Formulation and Digital Analysis in Close-Range Photogrammetry. Photogrammetric Engineering and Remote Sensing, Col. XLI, No. 11, pp. 1355-1373, 1975.

APPENDIX A

LINEARIZATION OF THE COLLINEARITY CONDITION

A.1 Linear forms of the collinearity condition

The observation equations 3.3 can be derived for any point j imaged on the photograph i as follows:

$$x_{ij} = F$$

$$y_{ij} = G \qquad \text{A.1}$$

Where: $$F = -f_i \frac{M_{1i} X_{ij}}{M_{3i} X_{ij}}$$

$$G = -f_i \frac{M_{2i} X_{ij}}{M_{3i} X_{ij}}$$

The linearization of Eq. A.1 is obtained by using approximate values for the unknown parameters and employing Taylor's series analysis,then it is obtained:

$$x_{ij} - V_{xij} = F_o + \dot{B}_{xij}\dot{\delta} + \ddot{B}_{xij}\ddot{\delta}$$

$$y_{ij} - V_{yij} = G_o + \dot{B}_{yij}\dot{\delta} + \ddot{B}_{yij}\ddot{\delta} \qquad \text{A.2}$$

Where: F_o , G_o are the values of F and G using approximations for the unknown parameters.

$\dot{B}_{xij}$ is a 6x1 row vector containing the partial derivatives of the F with respect to the orientation parameters of the camera station i.

$$\dot{B}_{xij} = \begin{bmatrix} \frac{\partial F}{\partial X_i} & \frac{\partial F}{\partial Y_i} & \frac{\partial F}{\partial Z_i} & \frac{\partial F}{\partial \omega_i} & \frac{\partial F}{\partial \phi_i} & \frac{\partial F}{\partial \kappa_i} \end{bmatrix}$$

$\ddot{B}_{xij}$ is a 3x1 row vector containing the partial derivatives of the F with respect to the ground coordinates of the observed point j.

$$\ddot{B}_{xij} = \begin{bmatrix} \frac{\partial F}{\partial X_j} & \frac{\partial F}{\partial Y_j} & \frac{\partial F}{\partial Z_j} \end{bmatrix}$$

$\dot{B}_{yij}$ is a 6x1 row vector given as:

$$\dot{B}_{yij} = \begin{bmatrix} \frac{\partial G}{\partial X_i} & \frac{\partial G}{\partial Y_i} & \frac{\partial G}{\partial Z_i} & \frac{\partial G}{\partial \omega_i} & \frac{\partial G}{\partial \phi_i} & \frac{\partial G}{\partial \kappa_i} \end{bmatrix}$$

$\ddot{B}_{yij}$ is a 3x1 row vector given as:

$$\ddot{B}_{yij} = \begin{bmatrix} \frac{\partial G}{\partial X_j} & \frac{\partial G}{\partial Y_j} & \frac{\partial G}{\partial Z_j} \end{bmatrix}$$

$\dot{\delta}_i$ is a 6x1 column vector containing the corrections to the approximate values of the orientation parameters of the camera station i.

$$\dot{\delta}_i = \begin{bmatrix} \Delta X_i \\ \Delta Y_i \\ \Delta Z_i \\ \Delta \omega_i \\ \Delta \phi_i \\ \Delta \kappa_i \end{bmatrix}$$

δ_j is a 3x1 column vector containing the corrections to the approximate values of the ground coordinates of the observed point j.

$$\ddot{\delta}_j = \begin{bmatrix} \Delta X_j \\ \Delta Y_j \\ \Delta Z_j \end{bmatrix}$$

It is convenient to make the subtitution:

$$\varepsilon_{xij} = x_{ij} - F_o$$

$$\varepsilon_{yij} = y_{ij} - G_o \qquad \text{A .3}$$

The equations A.2 can be farther simplified as follows:

$$V_{xij} + \begin{bmatrix} a_1 & a_2 & a_3 & a_4 & a_5 & a_6 \end{bmatrix} \dot{\delta}_i + \begin{bmatrix} a_7 & a_8 & a_9 \end{bmatrix} \ddot{\delta}_j = a_{10}$$

$$V_{yij} + \begin{bmatrix} b_1 & b_2 & b_3 & b_4 & b_5 & b_6 \end{bmatrix} \dot{\delta}_i + \begin{bmatrix} b_7 & b_8 & b_9 \end{bmatrix} \ddot{\delta}_j = b_{10} \qquad \text{A.4}$$

Where: $\begin{bmatrix} a_1 & a_2 & a_3 & a_4 & a_5 & a_6 \end{bmatrix} = \dot{B}_{xij}$

$$\begin{bmatrix} a_7 & a_8 & a_9 \end{bmatrix} = \ddot{B}_{xij}$$

$$a_{10} = \varepsilon_{xij}$$

$$\begin{bmatrix} b_1 & b_2 & b_3 & b_4 & b_5 & b_6 \end{bmatrix} = \dot{B}_{yij}$$

$$\begin{bmatrix} b_7 & b_8 & b_9 \end{bmatrix} = \ddot{B}_{yij}$$

$$b_{10} = \varepsilon_{yij}$$

It is obvious that:

$$a_1 = \frac{\partial F}{\partial X_i} \quad , \quad a_2 = \frac{\partial F}{\partial Y_i} \quad , \quad \ldots \quad a_6 = \frac{\partial F}{\partial \kappa_i}$$

$$a_7 = \frac{\partial F}{\partial X_j} \quad , \quad a_8 = \frac{\partial F}{\partial Y_j} \quad , \quad a_9 = \frac{\partial F}{\partial Z_j}$$

$$a_{10} = x_{ij} - F_o$$

$$b_1 = \frac{\partial G}{\partial X_i} \quad , \quad b_2 = \frac{\partial G}{\partial Y_i} \quad , \quad \ldots \quad b_6 = \frac{\partial G}{\partial \kappa_i}$$

$$b_7 = \frac{\partial G}{\partial X_j} \quad , \quad b_8 = \frac{\partial G}{\partial Y_j} \quad , \quad b_9 = \frac{\partial G}{\partial Z_j}$$

$$b_{10} = y_{ij} - G_o$$

The equations A.2 and A.4 can be reduced in one matrix equation (Brown, 1976):

$$V_{ij} + \dot{B}_{ij}\,\dot{\delta}_i + \ddot{B}_{ij}\,\ddot{\delta}_j = \varepsilon_{ij} \qquad 3.4$$

Where:

$$V_{ij} = \begin{bmatrix} V_{xij} \\ V_{yij} \end{bmatrix}$$

$$\dot{B}_{ij} = \begin{bmatrix} \dot{B}_{xij} \\ \dot{B}_{yij} \end{bmatrix}$$

$$\ddot{B}_{ij} = \begin{bmatrix} \ddot{B}_{xij} \\ \ddot{B}_{yij} \end{bmatrix}$$

$$\varepsilon_{ij} = \begin{bmatrix} \varepsilon_{xij} \\ \varepsilon_{yij} \end{bmatrix}$$

Notice the formulas A.2, A.4 and 3.4 are identical, they express the linear form of the collinearity condition and they differ in notation.

A.2 Evaluation of partial derivatives

The Eq.3.1 can be generally written as follows (Wolf, 1974):

$$x = -f\frac{r}{q}$$

$$y = -f\frac{s}{q} \qquad A.5$$

Where: $q = m_{31}(X_A-X_L) + m_{32}(Y_A-Y_L) + m_{33}(Z_A-Z_L)$

$r = m_{11}(X_A-X_L) + m_{12}(Y_A-Y_L) + m_{13}(Z_A-Z_L)$

$s = m_{21}(X_A-X_L) + m_{22}(Y_A-Y_L) + m_{23}(Z_A-Z_L)$

Considering Eq. A.1 then:

$$F = -f\frac{r}{q}$$

$$G = -f\frac{s}{q} \qquad \text{A.6}$$

Some quantities which are used for evaluating the partial derivatives are given as follows:

$$\frac{\partial q}{\partial \omega} = D_{11} = -m_{33}(Y_A - Y_L) + m_{32}(Z_A - Z_L)$$

$$\frac{\partial q}{\partial \phi} = D_{12} = \cos\phi(X_A - X_L) + \sin\omega\sin\phi(Y_A - Y_L) - \cos\omega\sin\phi(Z_A - Z_L)$$

$$\frac{\partial r}{\partial \omega} = D_{21} = -m_{31}(Y_A - Y_L) + m_{12}(Z_A - Z_L)$$

$$\frac{\partial r}{\partial \phi} = D_{22} = -\sin\phi\cos\kappa(X_A - X_L) + \sin\omega\cos\phi\cos\kappa(Y_A - Y_L) - \cos\omega\cos\phi\cos\kappa(Z_A - Z_L)$$

$$\frac{\partial s}{\partial \omega} = D_{31} = -m_{23}(Y_A - Y_L) + m_{22}(Z_A - Z_L)$$

$$\frac{\partial s}{\partial \phi} = D_{32} = \sin\phi\sin\kappa(X_A - X_L) - \sin\omega\cos\phi\sin\kappa(Y_A - Y_L) + \cos\omega\cos\phi\sin\kappa(Z_A - Z_L)$$

$m_{11} = \cos\phi\cos\kappa$

$m_{12} = \cos\omega\sin\kappa + \sin\omega\sin\phi\cos\kappa$

$m_{13} = \sin\omega\sin\kappa - \cos\omega\sin\phi\cos\kappa$

$m_{21} = -\cos\phi\sin\kappa$

$m_{22} = \cos\omega\cos\kappa - \sin\omega\sin\phi\sin\kappa$

$m_{23} = \sin\omega\cos\kappa + \cos\omega\sin\phi\sin\kappa$

$m_{31} = \sin\phi$

$m_{32} = -\sin\omega\cos\phi$

$m_{33} = \cos\omega\cos\phi$

The partial derivatives used in equations A.2 , A.4 and 3.4 are given as follows:

$$\frac{\partial F}{\partial \omega_i} = - \frac{f}{qq}(q\ D_{21} - r\ D_{11})$$

$$\frac{\partial F}{\partial \phi_i} = - \frac{f}{qq}(q\ D_{22} - r\ D_{12})$$

$$\frac{\partial F}{\partial \kappa_i} = - \frac{sf}{q}$$

$$\frac{\partial F}{\partial X_j} = - \frac{f}{qq}(q\ m_{11} - r\ m_{31}) = - \frac{\partial F}{\partial X_i}$$

$$\frac{\partial F}{\partial Y_j} = - \frac{f}{qq}(q\ m_{12} - r\ m_{32}) = - \frac{\partial F}{\partial Y_i}$$

$$\frac{\partial F}{\partial Z_j} = - \frac{f}{qq}(q\ m_{13} - r\ m_{33}) = - \frac{\partial F}{\partial Z_i}$$

$$\frac{\partial G}{\partial \omega_i} = - \frac{f}{qq}(q\ D_{31} - s\ D_{11})$$

$$\frac{\partial G}{\partial \phi_i} = - \frac{f}{qq}(q\ D_{32} - s\ D_{12})$$

$$\frac{\partial G}{\partial \kappa_i} = \frac{fr}{q}$$

$$\frac{\partial G}{\partial X_j} = - \frac{f}{qq}(q\ m_{21} - s\ m_{31}) = - \frac{\partial G}{\partial X_i}$$

$$\frac{\partial G}{\partial Y_j} = - \frac{f}{qq}(q\ m_{22} - s\ m_{32}) = - \frac{\partial G}{\partial Y_i}$$

$$\frac{\partial G}{\partial Z_j} = - \frac{f}{qq}(q\ m_{23} - s\ m_{33}) = - \frac{\partial G}{\partial Z_i}$$